

1 Catalina Eddy as Revealed by the Historical Downscaling of Reanalysis

2 Masao Kanamitsu and Elena Yulaeva

3 Scripps Institution of Oceanography, University of California, San Diego

4

5 February 7, 2011

6 Submitted to the *Journal of Geophysical Research, Atmospheres*

7

8

9

10

11

12

13

14

15

16

17

18

19 **Abstract**

20 Climatological properties, dynamical and thermodynamical characteristics, and
21 long-term variabilities of the Catalina Eddy are examined from the 61 year
22 NCEP/NCAR Reanalysis downscaled to hourly 10 km resolution. The eddy is
23 identified as a mesoscale cyclonic circulation confined to the Southern California Bight
24 region. Pattern correlation of wind direction against the canonical Catalina Eddy is used
25 to extract cases from the downscaled analysis. Validation against published cases, the
26 NCEP operational North American Mesoscale analysis, geostationary satellite images,
27 surface observations and buoy observations confirmed that the downscaled analysis
28 accurately reproduces Catalina Eddy events.

29 Large-scale features associated with Eddy events are characterized by zonal
30 wind at 500 hPa and a cutoff low positioned over southeastern California/southern
31 Nevada at 850 hPa, which enhances the northeasterly flow over Central California
32 below this level. Near the surface, the Catalina Eddy is characterized by a streak of
33 positive vorticity emanating from the coast of the Santa Barbara Channel, with two
34 centers, the southern one corresponding to the Eddy center. The eddy is associated with
35 convergence at the center and divergence along the coast. The temperature anomaly is
36 warm to the west and cold to the southeast. A positive humidity anomaly is apparent to

37 the east of the eddy, extending well into land. A vertical cross section indicates a
38 shallow vorticity structure reaching only up to 900 hPa. The thermal structure indicates
39 an eastward tilt with height.

40 A composite analysis of the initiation phase of the eddy indicates that no
41 apparent large-scale cyclonic/anti-cyclonic large-scale forcing is associated with the
42 eddy formation or decay. The source of the vorticity is located at the coast of the Santa
43 Barbara Channel. It is generated by the convergence of the wind system crossing over
44 the San Rafael Mountains and the large-scale northwesterly flow associated with the
45 subtropical high. This vorticity is advected towards the southeast by the northwesterly
46 flow which contributes to the formation of the streak of positive vorticity. At 6 hours
47 prior to the mature stage, there is an explosive generation of positive vorticity along the
48 coast, coincident with the phase change of the sea breeze circulation (wind turning from
49 onshore to offshore), resulting in the convergence all along the California coast. The
50 generation of vorticity due to convergence along the coast together with the advected
51 vorticity from the north resulted in the formation of southerly flow along the coast,
52 forming the Catalina Eddy. An examination of the surface pressure anomaly evolution
53 showed that vorticity is leading the eddy formation rather than the pressure gradient,
54 since no apparent formation of a south-to-north pressure gradient along the coast at the

55 initiation phase is recognized. Seven to eight hours prior to the mature stage, a strong
56 cold tongue forms along the southern California coast, and the surface pressure
57 increases in response to the cooling. The thermal structure indicates indirect circulation,
58 suggesting the conversion of eddy kinetic energy to eddy potential energy, implying that
59 the eddy kinetic energy is supplied from the large-scale northwesterly flow, but is
60 dissipated by potential energy conversion and surface friction.

61 The importance of diurnal variation and the lack of large-scale forcing are new
62 findings which are in sharp contrast to prior studies. These differences are due to the
63 inclusion of many short-lived eddy events detected in our study which have not been
64 included in other studies, aided by the hourly 10-km model output spanning 61 years.

65 Using extended historical analysis, the long-term behavior of the CE events is
66 examined. Although regression of the CE index onto surface temperature showed a La
67 Nina-like pattern, all the correlations were found to be insignificant. The correlations
68 with PDO, AO and ENSO indexes were also found to be small, suggesting weak
69 climate-scale control of CE activity by those modes.

70

71 **1. Introduction**

72 The Catalina Eddy (CE) is a formation of meso-scale cyclonic circulation along
73 the coast of southern California within a large-scale northeasterly flow associated with a
74 semi-permanent subtropical high pressure system. CE develops when the regular
75 northwesterly flow changes direction and turns to southerly flow along the California
76 coast, producing cyclonic circulation over the Southern California Bight. It has several
77 important meteorological implications including change in visibility, occasional
78 production of light rain, variation in pollution, and lowering of coastal temperature.
79 Some of the cloudy weather often associated with the CE is locally called “May gray”
80 or “June gloom” depending on the month of occurrence. It is an interesting
81 phenomenon dynamically, since the winds adjacent to the coast are directed towards the
82 opposite direction expected from the general large-scale pressure gradient.

83 A CE event is considered to be an instance of the occurrence of Coastally
84 Trapped Disturbances (Mass and Steenburgh, 2000), but it is differentiated by its
85 location and stationary nature in the Southern California Bight region. There are large
86 numbers of CE studies. Bosart (1983) was the first to conduct a comprehensive
87 synoptic analysis of an event using a limited number of observations, and to present the
88 evolution and possible mechanisms of its formation. His results were later confirmed

89 by several other studies, ranging from observational (Mass and Albright, 1989, hereafter
90 referred to as MA) to modeling (Davis, et al, 2000). The general nature of the CE and
91 its formation/decaying mechanisms is thought to be well understood. Currently well-
92 recognized characteristics of the CE are:

- 93 1) Eddies have a horizontal scale of about 100 km and vertical extension of
94 100-150 hPa.
- 95 2) The increase of stratus along the coast.
- 96 3) Most eddies are stationary, but occasionally have northward movement.
- 97 4) Events are associated with higher inversion layer.
- 98 5) The associated clouds extend well into land and prolong the cloudy state
99 into afternoon.

100 The dynamical mechanism is thought to be due to the effect of mountain wave
101 over the San Rafael Mountains which creates low pressure at the lee side of the
102 mountains, along the coast of the Santa Barbara Channel, triggering the eddy (Bosart
103 1983). The large-scale forcing that creates ridging along the coast, together with the lee
104 side trough, generates a south-to-north pressure gradient that forces the southerly flow
105 along the coast (Bosart, 1983; Clark, 1994; Reason and Steyn, 1992; Ulrickson et al
106 1995). Other theories suggest Kelvin wave formation due to the existence of a strong

107 inversion layer and a sudden change in large-scale forcing (Clark, 1994; Dormán, 1985;
108 Eddington et al, 1992). The decaying stage is associated with the weakening of the
109 along-shore pressure gradient due to the passage of synoptic disturbances. In all these
110 studies, large-scale forcing is one of the key controlling mechanisms.

111 Previous studies of CE events are mostly based on a few long lasting and well
112 pronounced cases. Bosart (1983) chose a case based on the satellite visible pictures.
113 Clark and Dembek (1991) utilized a special observation network together with GOES
114 satellite images. Wakimoto's (1987) analysis is based on a special observation program
115 with subjective surface pressure analysis. Kessler and Douglas (1991) also utilized a
116 special observation network to study the Eddy. Davis et al, (2000), Ueyoshi and Roads
117 (1993) and Ulrickson et al (1995) chose the Eddy case from MA. Only MA utilized a
118 large number of cases (about 50) to study the general characteristics of the CE events. It
119 should be emphasized that in their study, CE is not defined by identifying the cyclonic
120 circulation, but by a proxy, namely by the long-lasting strong southerly flow at San
121 Diego. Thompson et al (1997) utilized a typical large-scale pattern favorable for Eddy
122 formation from the MA study and identified the Eddy by actually running the numerical
123 simulation.

124 All these studies placed a strong constraint on the time scale of the eddy by

125 restricting its lifetime to 18 hours or longer, which may alter the general nature of the
126 CE if the eddy's lifetime is shorter. The application of proxy data used by MA may
127 contaminate the CE cases when a sub-synoptic disturbance unrelated to CE passes
128 through, or the coastal wind reversal develops without forming eddy circulation.
129 Simply identifying the Eddy from one-time satellite observation can be dangerous in
130 some instances. In addition, strong diurnal variation of the wind system along the coast
131 noted by MA may greatly modulate the Eddy, whose analysis requires hard-to-obtain
132 high temporal resolution observations. In fact, many of the uncertainties of CE studies
133 are due to the lack of proper high temporal and spatial observation networks.
134 Consequently, the characteristics and dynamical mechanisms of CE still have room for
135 further study.

136 The purpose of this paper is to utilize 57-year California Reanalysis
137 Downscaling at 10 km (CaRD10) resolution (Kanamitsu and Kanamaru, 2007;
138 Kanamaru & Kanamitsu, 2007), recently extended to 61 years, to examine the general
139 character of the Catalina Eddy and its possible formation mechanisms. This dataset
140 consists of hourly 10 km horizontal resolution outputs for the years 1948 to 2008, ideal
141 for the detection of Catalina Eddy events. The output provides various diagnostic fields,
142 suitable for dynamical and thermodynamical analysis of the eddy. The hourly output

143 also allows us to study the interaction between diurnal variation and Eddy activity. In
144 addition, the 61 years of analysis enable us to examine the interannual and long-term
145 trend of the Eddy activity.

146 This paper will be structured in the following manner. Section 2 briefly
147 describes CaRD10, Section 3 provides the eddy detection method and its verification,
148 Section 4 is devoted to the climatological characteristics of the Eddy, Section 5
149 examines the dynamical and thermodynamical features together with the formation
150 mechanism, and Section 6 describes long-term climatological features. The summary
151 and conclusions are given in Section 7.

152 **2. CaRD10**

153 CaRD10 is a dynamical downscaling of NCEP/NCAR reanalysis. The 6 hourly
154 200 km resolution Reanalysis is dynamically downscaled to hourly 10 km resolution
155 using the RSM (Regional Spectral Model, Juang and Kanamitsu, 1994). Spectral
156 nudging is applied to wind whose scale is greater than 1000 km (Kanamitsu et al, 2010).
157 Area average temperature at each level is also adjusted towards Reanalysis. Note that
158 the downscaling utilizes large-scale forcing only from reanalysis and no local
159 observations are used. Therefore, small-scale details, including meso-scale CE
160 circulations, are simply generated by the regional dynamics/physics of the model. The

161 RSM is a state-of-the-art atmospheric model with a comprehensive physics package.
162 Details of the RSM are found in Kanamitsu and Kanamaru (2007). The CaRD10
163 product has been verified against station observations and compared with North
164 American Regional Reanalysis (NARR, Mesinger et al., 2010), which utilized a data
165 assimilation system with local surface observations. It was shown that over the ocean,
166 CaRD10 near-surface wind analysis is as good as NARR, and it is superior over land
167 (Kanamaru and Kanamitsu, 2007) due mainly to the higher resolution of RSM (10 km
168 vs. 35 km for NARR).

169 **3. Eddy detection method**

170 CE events are defined as near-surface cyclonic circulation localized within the
171 bight of southern California and centered near Santa Catalina Island (see Figure 1 for
172 characteristic geographical features and major city locations over the area). A
173 composite of the wind field 10 m above the surface was used for CE events detection.
174 The canonical eddy was obtained by averaging fifteen typical events detected in both
175 CaRD10 and MA. Figure 2 shows the 15 events composite maps of the near-surface
176 relative vorticity and streamlines. The structure of the eddy is characterized by
177 elongated positive vorticity emanating from Point of Conception, with a narrow band of
178 negative vorticity along the coast.

179 The spatial pattern correlations between the composite near-surface wind
180 directions and the hourly CaRD10 10 m wind directions were then calculated within the
181 rectangular area 32°N – 34°N, 121° W- 117° W (area shown in Figure 2). Since we
182 were interested only in the wind directions and not in the amplitudes, we used the
183 Pearson product-moment correlation coefficient. We considered that a CE event
184 occurred if the correlation coefficient was larger than a certain threshold. We
185 intentionally did not segregate events by season, duration, or time of occurrence.

186 **3.1. Sensitivity to the value of the threshold**

187 Experiments to determine the sensitivity of the features of the detected eddy to
188 the correlation coefficient threshold were conducted. The composites of the initial
189 stages of the CE events for different threshold values were examined. Figure 3 displays
190 vorticity and wind detected with the threshold from 0.9 (upper left panel) to 0.1 (lower
191 right panel) in 0.1 increments. From subjective evaluation, a correlation of 0.7 which
192 presents significant cyclonic rotation over the Southern California bight, is selected for
193 the CE detection criteria. We note that most of the results obtained in this paper are not
194 very sensitive to the choice of this criterion, except for the distribution of the duration of
195 very short lasting events of about one hour.

196 **3.2. Validation**

197 Validations against other independent data sets were conducted. First we
198 compared CE events detected with our method to those from MA for May –September
199 1968-1982. MA used the sustained southerly surface wind of at least 1. m/s for at least
200 18 continuous hours at a San Diego land station as a proxy for the CE event. Table 1
201 shows hit and miss occurrences for this time period. The success rate is 80% indicating
202 that the dynamical downscaling is capable of reproducing CE events without injection
203 of local observations and confirms that our method is a reasonable tool for CE event
204 detection. Ueyoshi and Roads (1993), Skamarock et al. (2002) and Davis et al. (2000)
205 have demonstrated the capability of numerical models to reproduce typical CE. The
206 events that were missed by our detection methods were subjectively analyzed. Some of
207 them were merely coastally trapped disturbances without a notable rotational
208 component, and some others were baroclinic disturbances that happened to satisfy MA's
209 condition at San Diego, suggesting that our true CE detection rate is even higher.

210 In order to further validate our CE detection method, we used three
211 independent observations. First we applied the 4 km resolution GOES satellite imagery
212 data available for the period December 1995 to September 2008. Some of the cases are
213 well-validated by anomalous low cloud occurrence, but validation of all the eddy cases
214 was very difficult due to difficulties in recognizing eddy patterns from the imagery.

215 Secondly, we validated against the North American Mesoscale (NAM) Analysis data,
216 which consist of 12 km horizontal resolution data assimilation utilizing conventional
217 surface and buoy observations. The data is available in six hour intervals (00, 06, 12 and
218 18 UTC). 75% of CaRD10 CE events were also found in NAM. Thirdly, as an attempt
219 to validate the accuracy of the diurnal component of the CE detected in CaRD10, we
220 utilized hourly National Data Buoy Center data. For this validation, the duration of the
221 southerly wind events at San Diego Scripps Pier, used as a proxy of eddy formation by
222 MA, is examined. Figure 4 shows PDFs of the duration of such events by hour. In the
223 Scripps Pier data, the short-lived southerly wind occurred nearly twice as often as in the
224 CaRD10 data, suggesting that the CaRD10 may even be underestimating the existence
225 of very short-lived Eddy events, but the relation between the Scripps Pier data and the
226 existence of CE is not certain for these very short-lived southerly events.

227 With these extensive comparisons to independent datasets, we are confident
228 that the CaRD10 dynamically downscaled analysis detects Catalina Eddy with
229 reasonable accuracy.

230 **4. Climatological characteristics**

231 Analysis of 61 years of CaRD10 Catalina Eddy events, summarized in Figure
232 5, revealed that the CEs appear most frequently in the May-June period when the eddies

233 are strongest in terms of vorticity (Fig. 5a and b). The maximum intensity eddy in terms
234 of vorticity is observed at 16 UTC, 8:00 a.m. local Pacific Standard time (Fig. 5d). The
235 average duration of the mature stage (defined as the wind direction correlation with
236 canonical CE greater than 0.7) is about 4.4 hours (Fig 5c), but a large number of eddies
237 have a mature stage shorter than 1 hour (Fig. 5d). When the threshold correlation for
238 CE detection is lowered to 0.5, the number of eddies with a mature stage shorter than 1
239 hour increases. Mature stage eddies lasting longer than 18 hours are very rare,
240 accounting for only a small percent of all the CEs detected. This is in sharp contrast to
241 previous works which are based on long-lasting and relatively rare very strong cases.
242 The relatively short average mature stage duration obtained in this study is somewhat
243 surprising. Considering the underestimation of San Diego offshore southerly wind
244 events in CaRD10 compared with offshore buoy observation mentioned in Section 3.1,
245 the actual number of eddies may be even larger and their mature stage duration may be
246 even shorter.

247 The reason for the short mature stage duration is further examined by looking
248 at an hourly evolution of eddies. Figure 6 shows an example of a short-lived eddy case
249 observed during April 30 and May 2, 2000. The eddy appeared consecutively for three
250 days at a particular local time, but it tended to weaken and disappear during 21 UTC to

251 03 UTC (1:00 p.m. to 7:00 p.m. local time). The hourly resolution CaRD10 output
252 makes it possible to identify this strong diurnal variability in the eddy activity. We
253 believe this intermittency is a reason for the relatively short mature stage duration
254 obtained in this analysis. The duration of mature stage CE can be aliased to a longer
255 lasting eddy if any of the observations are missing during 21 UTC to 03 UTC, or if the
256 relation between southerly wind in San Diego and Eddy formation breaks down. One
257 may notice that the slight southerly component at the San Diego location (indicated by a
258 white circle in the top left panel) is observed even when the CE dissipates, suggesting
259 the possible breakdown of the relationship between winds at San Diego and CE, leading
260 to the erroneous overestimation of eddy lifetime. Unfortunately, the evolution of CE
261 shown in Fig. 6 could not be verified against observations due to missing hourly station
262 data over the bright area. In order to further strengthen our argument, we show another
263 case with hourly station observation in Figure 7 (September 17-18, 2007). We see a
264 dissipating eddy at 01 UTC which is supported by several observations, but the eddy
265 reappears after 8 hours at 09 UTC.

266 The hour of the establishment of the mature stage and the maximum intensity
267 during the day are shown in Fig. 5e. In terms of the pattern correlation, the maximum
268 number of cyclonic circulations are observed at around 08-13 UTC (0:00 a.m. to 4:00

269 a.m. local time). The eddy reaches its maximum intensity, as measured by positive
270 vorticity amplitude, during 13-19 UTC (5 a.m. to 11a.m. local time). A more detailed
271 timeline of the CE life cycle will be discussed later.

272 Figure 8 shows the large-scale anomaly patterns at 500 and 850 hPa associated
273 with the mature phase of the CE. At 500 hPa, the typical pattern is the low anomaly to
274 the north and elongated strong positive anomaly extending from the western extra-
275 tropical Pacific towards inland, passing just north of Point Conception (Fig. 8a). The
276 full field map shows that the geopotential height field is nearly zonal with a very weak
277 horizontally tilted trough oriented from 33N, 114W to 18N, 120W (Fig 8c), suggesting a
278 lack of strong large-scale cyclonic/anti-cyclonic forcing at least at this level. At 850
279 hPa, the negative anomaly extends southward over the land and a positive weak
280 anomaly over the western extra-tropics without clear ridging extension (Fig.8b) can be
281 seen. The anomalous wind is generally north-north-westerly over the entire domain
282 except over the southwestern portion. The full field map shows generally high
283 geopotential over the southeastern portion of the Pacific and low geopotential over the
284 continent, producing a pressure increase from southwest to northeast (Fig. 8d). The
285 anomaly patterns at these two levels agree well with MA, but the amplitudes of the
286 ridges and troughs are much weaker. The anomaly at 850 hPa enforces wind flowing

287 across the San Rafael Mountains, which is a key to the generation of the CE, as detailed
288 in the following sections (also noted by all the previous studies).

289 Figure 9 (left panel) describes the main characteristics of the mature phase of
290 the CE anomaly composite. Note that the anomalies in this paper are computed by
291 subtracting the 57-year mean of the field at a fixed local time to eliminate the
292 climatological diurnal variability appearing in the anomaly field. The composite near-
293 surface structure of the eddy is characterized by elongated positive vorticity emanating
294 from the Point of Conception, with a narrow band of negative vorticity along the coast.
295 The location of the center of the positive vorticity coincides with the circulation center,
296 which is not the case in the composite eddy used for detection. There are two vorticity
297 maxima and minima roughly aligning east-west in pairs. The negative vorticity center
298 located just over the Santa Monica Mountains is more conspicuous, stronger and is
299 located to the south of the eddy composite used for detection (Figure 2). This negative
300 vorticity center enhances the onshore flow to the north, separating the positive vorticity
301 streak from Point of Conception into two maxima. It appears to be more distinct at
302 upper levels, clearly seen as anticyclonic eddy at 925 hPa (Fig. 9 right panel). This
303 anticyclonic circulation seems to be forced by the underlying geographical features of
304 the Santa Monica Mountains.

305 There is a surface convergence associated with the eddy (Fig. 10 left panel)
306 with the accompanying large areas of divergence to the east and northeast of the eddy.
307 Away from the eddy areas, areas of divergence anomaly are evident over the upslope
308 wind areas of the northern San Rafael Mountains. A belt of convergence along the coast
309 of the Santa Barbara Channel to the north of Los Angeles is the result of accelerating
310 down-slope wind from the mountains (or the lee wave) colliding with the northerly flow
311 associated with the CE. Near-surface temperature is colder to the east of the eddy
312 center and warmer to the west (Fig. 10, right panel), resembling the middle-latitude low
313 but with a completely opposite temperature structure, i.e., warm to the west and cold to
314 the east. Compared to the divergence field (Fig. 10, left) we see that the relatively cold
315 air is converging and rising and warm air is diverging and sinking, suggesting the
316 conversion from kinetic energy to potential energy.

317 There is a very warm anomaly area to the north of the CE, over the San Rafael
318 Mountains along the Santa Barbara Channel coastline. The warm area is located over
319 the mountain slopes with down-slope winds, suggesting the effect of adiabatic warming
320 caused by large-scale forcing consistent with the 850 hPa height and wind anomaly
321 (Fig. 8). The warm down-slope wind area along the Santa Barbara Channel is
322 indicative of the mountain effect, first described by (Bosart, 1983) and later by many

323 others (Davis et al 2000; Skamarock et al 2002; Thompson et al 1997 ; Ulrickson et al
324 1995). Interestingly, southwest of Los Angeles in the San Diego Coastal Range (see
325 Fig. 1), a warm area is associated with the up-slope wind, suggesting the diabatic
326 heating control. This is a good demonstration of different thermal and dynamical
327 mechanisms working in a small scale. The moisture anomalies show increased specific
328 humidity as well as increased relative humidity to the east of the Eddy, extending inland
329 (Fig. 11), indicating the intrusion of stratus farther into land. Latent heat flux is
330 decreased by more than 25 W/m^2 along the vorticity center due to weaker winds (see
331 Fig 12). This reduced evaporation may compensate the reduction in incoming solar
332 radiation due to increased cloudiness. Further study utilizing a regional coupled model
333 could yield interesting CE air-sea interaction. The SLP pattern exhibits the low
334 pressure located at the center of the eddy circulation (Fig. 13) with a trough extending to
335 the Santa Barbara Channel coast. The ridging along the southern California coast is
336 distinct. Clark (1994), Reason and Steyn (1992), Eddington et al (1992), Thompson et
337 al (1997), and Ulrickson et al (1995) consider this feature to be the key factor of the
338 initiation of the eddy.

339 The vertical cross sections of the eddy (Figure 14 right panel) show that the
340 positive vorticity anomaly extends to about 900 hPa. The negative vorticity to the east

341 of the eddy extends further into the 800 hPa level. The warm anomaly at around 950
342 hPa just above and west of the center is a very distinct thermal structure. A cold
343 anomaly exists to the east of the eddy center. Both warm and cold temperature
344 anomalies extend to 800 hPa. The thermal structure is not symmetric with respect to the
345 center of the eddy exhibiting an eastward vertical tilt, contrary to the middle latitude
346 disturbances.

347 **5. Development mechanism**

348 In this section the initiation phase is studied. In order to eliminate overlapping
349 events, we repeated analysis only for CE events separated by 24 or more hours from
350 other events. For this reason we avoided examining the decay phase, since 24 hour
351 separation can be contaminated by the initiation phase of the following CE event.
352 Figure 15 shows Z500 and Z850 fields at 21, 18, 15, 12, 9, 6, 3, and 1 hours before the
353 detection of a CE event, i.e. the start of the mature stage. Interestingly, there is very
354 little change in the 500 hPa height field prior to the CE formation, except for a slight
355 increase in the meridional gradient as the CE forms. This lack of large-scale
356 cyclonic/anticyclonic forcing during the initiation phase is in sharp contrast to MA and
357 other studies, in which large-scale forcing is found to be essential for initiation. This
358 result is due to the inclusion of many weak CE events in the current study, but

359 demonstrates that a weak CE can form without large-scale cyclonic/anti-cyclonic
360 forcing.

361 At 850 hPa, the situation is very much the same but an increase in the
362 intensity of the low over the Southeastern California/Southern Nevada region is noted,
363 which contributes to the increase of wind over the San Rafael Mountains by enforcing
364 the northerly flow. Figure 16 shows the near-surface anomaly wind vector and anomaly
365 vorticity during the initiation phase. At 21 hours before the mature stage, we see a small
366 area of positive vorticity located along the Santa Barbara Channel coast. The average
367 time of the full development phase is about 12 UTC (4:00 a.m. local time), thus, 21
368 hours before the full development stage corresponds to 15 UTC or 7:00 a.m. local time.
369 This vorticity maxima gradually intensifies and expands with time, and between 6 to 9
370 hours prior to the full development stage (03-06 UTC or 7:00 p.m.-10:00 p.m. local
371 time), there is explosive growth. At 3 hours prior (09 UTC or 1:00 a.m. local time), an
372 area of negative vorticity appears along the coast just to the east of the eddy which
373 eventually deforms the positive area to a shape resembling the sole of a shoe. This
374 combined positive and negative vorticity region resulted in the formation of southerly
375 flow along the coast. The figure indicates that the origin of the eddy is at the coast of
376 the Santa Barbara Channel. Over this area, the streamline has cyclonic curvature due to

377 the flow around the San Rafael Mountains. The strong convergence of the streamline is
378 associated with the flow crossing over the mountain. A northeasterly anomaly over
379 ocean is also clearly observed. These features are commonly pointed out in all the
380 previous Catalina Eddy studies.

381 In order to examine the growth of the positive vorticity maxima, a vorticity
382 budget calculation is performed from composite maps. Figure 17 shows major vorticity
383 budget terms at various stages of initiation. We identified two controlling terms, a
384 stretching term and horizontal advection term. 21 hours before the mature phase (15
385 UTC or 7:00 a.m. local time), positive vorticity along the Santa Barbara Channel coast
386 is caused by the stretching term due to the convergence. The generated vorticity is
387 advected southeast by the quasi-stationary northwesterly flow. A very similar
388 description of the event is presented by Davis et al (2000). The local time change of
389 vorticity is relatively small, indicating that the generated and advected vorticity is
390 dissipated by the surface friction. At 12 hours prior to the full development phase (00
391 UTC or 4:00 p.m. local time), vorticity generation by the stretching term extends south
392 along the coast. Horizontal advection further stretches the area of the positive vorticity
393 anomaly southward along the coast. Thus, the major source of vorticity is still located
394 along the coast of the Santa Barbara Channel. 6 hours prior to CE detection (06 UTC

395 or 10:00 p.m. local time), generation of positive vorticity due to the stretching term
396 suddenly spreads all along the coast. This hour is found to correspond to the time when
397 the diurnal variation of wind causes the wind to turn from onshore to offshore flow
398 along the entire west coast, generating a convergence line along the coast. The diurnal
399 evolution of the wind is shown in Figure 18. The blue area (negative zonal wind, i.e.
400 easterly wind) develops all along the coast at 6 hours prior to the full development
401 stage, which continues for at least the next 6 hours. Apparently, this transition causes
402 strong convergence just a few kilometers offshore of the Bight. The positive
403 contribution of the stretching term is widespread over the entire Southern California
404 coast. Small (1999) noted the effect of coastal convergence on the Catalina Eddy.
405 Previous studies indicate that the effect of sea breeze is unimportant (Skamarock et al,
406 2002), or important but not crucial for eddy initiation (Davis et al, 2000; Ulrickson et al,
407 1995), which contradicts our results. Very close to the coast, horizontal advection by
408 the offshore flow creates an area of negative vorticity which intensifies as it approaches
409 the full development phase.

410 We comment here that the disappearance of the CE during 21 UTC and 03
411 UTC presented in Section 4 (Figs. 5 and 6) corresponds to the diurnal phase of onshore
412 flow receding to offshore flow, when the convergence is rapidly taken over by

413 divergence, weakening and dissipating the eddy. Thus diurnal variation also seems to be
414 crucial to the decay phase.

415 The evolution of the thermal structure during the initial stage of the CE is
416 shown in Figure 19. The anomaly near-surface air temperature evolution indicates
417 expansion of the warm area from the north, again emanating from the coast of the Santa
418 Barbara Channel. It gradually expands southeastwards for the period of 20 to 11 hours
419 prior to the full development stage due to advection by northwesterly flow over ocean.
420 This is similar to the evolution of vorticity, but directing towards the west side of the
421 eddy rather than to the center of the vortex since the interaction between temperature
422 and wind is weaker than that between vorticity and wind. The warm air to the east of
423 the Eddy center is a very clear signal of full development eddy from the cross section
424 map, already shown in Figure 14. About 10 hours prior to the full development stage, a
425 strong cold anomaly develops at the southwestern corner of the domain and extends
426 towards the east side of the eddy along the coast, reaching its maximum intensity at the
427 full development stage. The formation of a cold tongue along the coast is also noted in
428 the numerical simulation by Ulrickson et al (1995), who explained the cause as the
429 result of blocking of westerly and northwesterly wind over the bight combined with the
430 general warming to the west of the eddy. Corresponding to this cooling, a surface

431 pressure ridge forms along the southern California coast. This sequence of events
432 suggests that the north to south pressure gradient is not the mechanism of the Eddy
433 formation, but is rather its consequence. Except for the cold anomaly along the coast to
434 the south of the eddy, the temperature field more or less goes back to the stage 20 hours
435 prior.

436 Full field maps revealed (not shown) an intrusion of warm air from the south
437 towards the Eddy for the 20 to 11 hours prior to the full development stage but this
438 warm air intrusion considerably weakens during the last 10 hours, creating the strong
439 cold anomaly along the coast to the south of the eddy. By the time the full
440 development stage is reached, the warm near-surface temperature anomaly along the
441 coast of the Santa Barbara Channel weakens.

442 In summary, from the vorticity budget view, the CE is initiated by the
443 stretching term due to the convergence caused by the flow across and around the San
444 Rafael Mountains. The generated vorticity is advected southward by the large-scale
445 wind associated with the subtropical high and dissipates due to surface friction at the
446 very early stages. As the generation by convergence continues, about 6 hours before the
447 full development phase, sudden generation of vorticity due to stretching occurs along
448 the entire west coast. This is caused by the convergence due to the turning of offshore

449 to onshore flow associated with diurnal variation. The vorticity at the CE center
450 increases due to advection from the north and generation along the coast. At this time,
451 the CE takes its characteristic shape. At the same time, very close to the coastline,
452 negative generation of vorticity takes place due mainly to horizontal advection of
453 negative vorticity from land. The maximum negative vorticity center appears over the
454 Santa Monica Mountains. This negative vorticity tends to separate the streak of
455 vorticity maximum emanating from the Santa Barbara Channel coast into two centers,
456 creating the shoe-sole shaped positive vorticity area. The location of the negative
457 vorticity center positioned at the arch of the sole corresponds well to the Santa Monica
458 Mountain region, suggesting the effect of local small-scale topographic features.

459 The thermal structure indicates the importance of the down-slope wind along
460 the coast of the Santa Barbara Channel, causing a warm anomaly from adiabatic
461 heating. This warm air is advected towards the southeast by the large-scale
462 northwesterly flow, causing a warm anomaly to the west of the Eddy center. At the fully
463 mature stage, a cold anomaly area appears along the southern coast.

464 Figure 20 shows hourly variation of surface pressure anomaly during the
465 initiation phase. 20 hours prior to the full development stage, there is a broad area of
466 low pressure anomaly over the entire Bight, which gradually deepens until 13 hours

467 prior when a small low pressure center area appears at the northern part of the Bight.
468 We do not see any low pressure area along the coast of the Santa Barbara Channel. The
469 low pressure center is located at the area with strong cyclonic curvature and diffluent
470 streamlines. The low pressure area gradually spreads towards southeast. At 10 hours
471 prior, an eddy center becomes recognizable at the western portion of the Santa Barbara
472 Channel coast. The low pressure area does not correspond to the center of the eddy, but
473 is located to the south/southeast, presenting the direction of movement of the eddy
474 center. The low pressure anomaly deepens further and at 6-5 hours prior, the eddy
475 center moves southeastwards and the pressure center starts to collocate with the eddy
476 center. The eddy further strengthens in harmony with the deepening of the low pressure
477 center afterwards. This wind-surface pressure anomaly relation shows that there is a
478 dominant ageostrophic component at the early stage, but the wind-pressure relationship
479 suggests that pressure is not driving the wind since the wind is not directing towards the
480 low pressure. Rather, the pressure anomaly seems to indicate the direction of the
481 movement of the Eddy at the early stage. This is in contrast with the Bosart (1983) and
482 MA interpretations of the development of the coastal southerly flow, which emphasize
483 the south to north pressure gradient as a driving mechanism. In our analysis, there is no
484 apparent north-south pressure gradient anomaly that drives the southerly flow, except at

485 the mature stage when the surface pressure ridge forms along the southern California
486 coast.

487 Figure 21 summarizes the life cycle of CE in relation to local time, together
488 with its relation to sea-breeze circulation. Some of the sample cases discussed in this
489 paper are also indicated. The rough estimate of the eddy's lifetime is 19 hours. The
490 eddy develops abruptly in the early evening and reaches the mature stage by midnight,
491 maintains its intensity until early morning, and then decays in the late afternoon, often
492 completely disappearing. The eddy is initiated when the phase of the sea-breeze turns
493 from onshore to offshore, and it decays during the opposite phase.

494 The current analysis suggests that the source of the eddy is the vorticity
495 generated by the convergence along the coast of the Santa Barbara Channel, which is
496 advected to the southeast to the Bight region, interacting with the vorticity generation
497 along the coast due to coastal convergence caused by the turning of the wind from
498 onshore to offshore sea breeze circulation. The event is vorticity driven rather than
499 pressure driven.

500 Looking at the thermal structure and convergence pattern, CE has a weak
501 baroclinic structure with temperature and vertical motion anomaly relationships,
502 convergence over a cold anomaly and divergence over a warm anomaly, indicating the

503 conversion of eddy kinetic energy to eddy potential energy. This implicitly indicates
504 that the CE's source of eddy kinetic energy comes from large-scale flow associated with
505 the sub-tropical high.

506 **7. Long-term climatological behavior**

507 The 57-year CaRD10 analysis and its extension allow for investigation of the
508 long term variability of CE events, which will be described in this section. In order to
509 characterize CE activity, we examined 4 indices; the monthly mean of vorticity
510 averaged over the CE region (shown in Figure 2), the monthly averages of wind
511 correlations used to detect the CE over the same region, the number of events per month
512 and the number of hours of observed CE per month. All these four indices are highly
513 correlated with each other with the lowest correlation being 0.64. Figure 22 compares
514 the first two CE indices, with a correlation coefficient of 0.75. The figure shows there is
515 very little long-term trend in the index, but some tendency of increase after 1990 may be
516 noted.

517 The temporal spectral analysis (Figure 23) of the vorticity averaged over the
518 area used above exhibits peaks corresponding to annual cycle, 10-year cycle and 26-day
519 cycle. The well known 26-day atmospheric cycle is the Yanai wave or the mixed
520 Rossby gravity wave in the tropics. In ocean, the 26-day cycle is observed in the

521 tropical Indian Ocean (Luyten, J. R., 1882) . The Tropical Instability Wave (Willett, et
522 al 2006) also has a periodicity of 20-40 days. However, all these waves are tropical in
523 origin, and their role in sub-tropical latitudes has not yet been identified. The 10-year
524 cycle probably corresponds to the PDO and is briefly discussed below.

525 The large-scale pattern associated with frequent eddy events is shown in Figure
526 24, presenting a strong ridging of anomaly over the west coast, corresponding to a more
527 zonal pattern. Near-surface temperature resembles a La Nina type of pattern, but
528 correlations do not exceed 0.3. These low correlation values are also found in the
529 individual correlations between low-frequency variability indices; ENSO correlation is
530 about -0.12, PDO correlation is about 0.05, and AO correlation is about 0.1 without lag,
531 and lower correlations with lags. We tentatively concluded that the relations between
532 CE events and low frequency variabilities were not significant, and predicting the year-
533 to-year variation of CE events is very difficult.

534 **8. Summary, discussions and conclusions**

535 Climatological properties, dynamical and thermodynamical characteristics, and
536 long-term variabilities of the Catalina Eddy (CE) are examined from the 61 year
537 NCEP/NCAR Reanalysis downscaled to hourly 10 km resolution. The eddy is
538 identified as a cyclonic circulation confined in the Southern California Bight region.

539 Pattern correlation of wind vector from canonical CE is used to extract cases from the
540 downscaled analysis. Validation against published cases, the NCEP operational North
541 American Mesoscale Analysis, geostationary satellite images, surface observations and
542 buoy observations are made and confirm that the downscaled analysis accurately
543 reproduces Catalina Eddy events.

544 In this study, 4136 Eddy events with 16769 total mature stage hours were
545 identified during the 61 years. This is 3% of the total hours in 61 years. The detailed
546 dynamical and thermodynamical features of the Eddy were examined by compositing
547 these cases during the initiation and mature phases.

548 The large-scale features associated with the Eddy formation comprise a zonal
549 flow at 500 hPa and a horizontally tilted trough oriented from Northeast to Southwest
550 over the continent with low pressure over the Southern California/Southern Nevada area
551 at 850 hPa. The 850 hPa anomaly enforces the north-northeasterly flow over the San
552 Rafael Mountain region which has been identified as crucial for the initiation of the CE.

553 The favorable months for eddy formation are May and June, while the least
554 formation occurs during the winter months. The strongest CEs appear in June. We
555 found that the CE events are more frequent than the previous studies suggested, since
556 those studies chose only strong events. There are very few CEs that maintain their full

557 strength longer than 18 hours. The average duration of the full strength of a CE is of the
558 order of 4-5 hours. The relatively short duration of the mature stage in this analysis is
559 due to the use of hourly output, which shows interruption of the eddy by the onshore sea
560 breeze circulation during the late afternoon to early evening (around 4 p.m. to 6 p.m.)
561 local time. This interruption may have been missed in previous studies due to the lack
562 of surface observations necessary to directly identify the cyclonic circulation within the
563 Bight region. The eddy intensity is strongest in the early morning at around 4:00 a.m.
564 local time.

565 The climatology of the mature phase of the eddy has the following
566 characteristics. A streak of vorticity emanating from the coast of the Santa Barbara
567 Channel is separated into two centers by a strong small-scale negative vorticity center
568 located over the Santa Monica Mountains. The southern vorticity maximum
569 corresponds to the center of the Catalina Eddy. The vorticity along the coast is
570 generally negative. The most prominent divergence feature is the strong divergence
571 over the northern slope of the San Rafael Mountains, paired with the strong
572 convergence over the southern slope. The region of positive vorticity streak and the
573 center of the eddy are associated with convergence. Other notable areas of divergence
574 are just off the coast of the Point of Conception and along the coast of Southern

575 California to the southeast of the eddy center. The temperature anomaly is warm to the
576 west and north of the eddy center, and cold to the west and southwest. There is an area
577 of very warm anomaly along the southern downslope region of the San Rafael
578 Mountains. The moisture anomaly shows an increase over the eastern part of the Eddy,
579 extending well into land, suggestive of the increase in cloudiness. Evaporation from the
580 surface is reduced at the center and to the east of eddy (but offshore) due to reduced
581 wind speed. Far offshore over the ocean not affected by eddy, evaporation is increased
582 due to increased wind speed, suggesting the possible importance of local air-sea
583 interaction. The surface pressure anomaly is in geostrophic balance with the near-
584 surface streamline, with minimum pressure coinciding with the eddy center. The
585 vertical extent of the eddy reaches only to 900 hPa as shown by previous researchers.
586 The thermal structure is warm to the west of the eddy and cold at the eddy center and to
587 the east. This thermal structure is in agreement with Ulrickson et al. (1995).
588 Temperature anomalies reach 800 hPa. The thermal structure is not symmetric,
589 suggesting an eastward tilt with height.

590 The analysis of the development stage of the eddy from composite maps shows
591 that the large-scale 500 hPa pattern does not change very much during the initiation,
592 except for the strengthening of the low located at southeastern California/southern

593 Nevada at 850 hPa. This geopotential height anomaly tends to enhance north-north
594 easterly flow across the San Rafael Mountains. The vorticity anomaly maximum is
595 located at the coast of the Santa Barbara Channel 20 hours prior to the fully developed
596 stage, slowly expanding along the coast, with explosive development at around 6 hours
597 prior to the mature stage. The vorticity budget indicated that the positive anomaly along
598 the Santa Barbara Channel coast is caused by the stretching term due to convergence
599 associated with the flow crossing over the San Rafael Mountains. This vorticity is
600 advected by large-scale northwesterly flow, but its magnitude is not large enough to
601 form a cyclonic circulation. About 6 hours prior to the start of the mature stage, there is
602 a strong generation of vorticity due to the stretching term all along the coast. This
603 stretching is caused by coastal convergence due to the phase change of the sea-breeze
604 circulation turning from onshore to offshore. Ulrickson et al. (1995) noted that sea-
605 breeze circulation simply delays the occurrence of the Eddy. Davis et al (2000) noted
606 the importance of sea-breeze. Clark and Dembek (1991) noted strong interaction
607 between the sea-breeze and CE. However, none of these studies noted the critical
608 importance of the sea-breeze circulation in initiating the CE. Our analysis clearly
609 indicated that the phase change of the sea-breeze circulation is essential for eddy
610 formation and decay.

611 The difference in the importance of the sea-breeze can be traced back to the
612 difference in large-scale forcing between the current and previous studies. Our
613 composite study indicated that the large-scale cyclonic/anticyclonic forcing was not
614 necessary for the eddy formation, while all the previous studies focused on the strong
615 eddy and concluded that the large-scale forcing is crucial. Our study suggests that the
616 eddy will form without strong large-scale forcing, and in this situation, sea-breeze
617 becomes essential for the control of the evolution of the eddy. Under strong large-scale
618 forcing, it is most likely that the effect of the sea-breeze circulation on eddy evolution
619 becomes secondary.

620 The near-surface thermal structure of the eddy evolves with a warm anomaly located
621 at the coast of the Santa Barbara Channel due to descending air along the San Rafael
622 Mountains forced by 850 hPa northeasterly winds. This warm air is advected southward
623 by the large-scale northwesterly flow. Because of the weaker interaction between
624 temperature and wind field compared to that between vorticity and wind, the warm air
625 tends to spread over the area to the west of the eddy center, creating the warm anomaly
626 there. The downward motion due to the acceleration of northwesterly flow off the Point
627 of Conception may also contribute to the warming. On the contrary, a cold anomaly
628 develops to the south and southeast of the eddy along the coast. This is probably due to

629 the increased vertical mixing caused by the rise of the top of the boundary layer
630 associated with the blocking of westerly winds by coastal mountains to the south of the
631 Eddy, combined with the general warming to the west of the eddy as suggested by
632 Ulrickson et al., (1995). These advection and vertical circulations are responsible for
633 the formation of the asymmetric thermal structure, as well as the north to south pressure
634 gradient along the coast. Although previous researchers argued that the eddy is initiated
635 by the surface pressure gradient along the coast, this study seems to indicate that the
636 pressure gradient is a result rather than a cause of the eddy formation, although as
637 argued by Ulrickson et al. (1995), the surface pressure gradient may act as a mechanism
638 to maintain the southerly flow along the coast after its formation. Our analysis seems to
639 indicate that the pressure pattern is determined by the eddy circulation and not the
640 reverse. This difference of the role of pressure gradient along the coast may also be
641 related to the differences in the strength of eddies studied in this and previous studies. It
642 is probable that in order to maintain the eddy for more than 18 hours, it is essential to
643 maintain a north to south pressure gradient by large-scale forcing.

644 The relation between divergence and temperature anomaly shows that the
645 relatively warm air is sinking to the west of the eddy and cold air is rising at the eddy's
646 center and to the east, implying energy conversion from eddy kinetic to eddy potential

647 energy. This conversion also implicitly indicates that the eddy kinetic energy is
648 generated from large-scale northeasterly flow, dissipated through kinetic to potential
649 energy conversion, together with the effect of surface friction.

650 Finally, the trend, inter-annual and inter-decadal variabilities of the CE
651 activities are examined. The temporal spectra of the vorticity averaged over the target
652 area shows peaks at 10 years, 1 year and 26 days. Regression of the CE index onto
653 monthly mean 500 hPa height indicates strong ridging in the anomaly over the west
654 coast, indicating the dominance of the zonal flow. Similar regression onto monthly
655 mean near-surface temperature showed a La Nina-like pattern with a warm anomaly
656 located over the west coast. Unfortunately, the correlation between PDO, AO and
657 ENSO indices are found to be very low, of the order of 0.1-0.2, suggesting that the
658 large-scale control of CE is weak except for the local positive anomaly at 500 hPa.

659

660 **References**

661 Bosart, L. (1983), Analysis of a California Catalina Eddy Event, *Mon. Wea. Rev.*, *111*,

662 1619-1633.

663 Clark, J. (1994), The Role of Kelvin Waves in Evolution of the Catalina Eddy, *Mon.*

664 *Wea. Rev.*, *122*, 838-850.

665 Clark, J., and S. Dembek (1991), The Catalina eddy event of July 1987: A Coastally

666 Trapped Mesoscale Response to Synoptic Forcing, *Mon. Wea. Rev.*, *119*, 1714-

667 1735.

668 Davis, C., S. Low-Nam, and C. Mass (2000), Dynamics of a Catalina Eddy Revealed by

669 Numerical Simulation, *Mon. Wea. Rev.*, *128*(8), 2885-2904. doi: 10.1175/1520-

670 0493(2000)128<2885:DOACER>2.0.CO;2.

671 Dormán, C. (1985), Evidence of Kelvin Waves in California's Marine Layer and

672 Related Eddy Generation, *Mon. Wea. Rev.*, *113*, 827-839.

673 Eddington, L. W., J. J. O'brien, and D. W. Stuart (1992), Numerical Simulation of

674 Topographically Forced Mesoscale Variability in a Well-Mixed Marine Layer,

675 *Mon. Wea. Rev.*, *120*, 2881-2896.

- 676 Juang, H. -M. H., and M. Kanamitsu (1994), The NMC Nested Regional Spectral
677 Model, *Mon. Wea. Rev.*, *122*, 3-26.
- 678 Kanamaru, H., and M. Kanamitsu (2007), Fifty-Seven-Year California Reanalysis
679 Downscaling at 10 km (CaRD10). Part II: Comparison with North American
680 Regional Reanalysis, *J. Climate*, *20*(22), 5572-5592. doi:
681 10.1175/2007JCLI1522.1.
- 682 Kanamitsu, M., and H. Kanamaru (2007), Fifty-Seven-Year California Reanalysis
683 Downscaling at 10 km (CaRD10). Part I: System Detail and Validation with
684 Observations, *J. Climate*, *20*(22), 5553-5571. doi: 10.1175/2007JCLI1482.1.
- 685 Kanamitsu, M., K. Yoshimura, Y. -B. Yhang, and S. -Y. Hong (2010), Errors of
686 Interannual Variability and Trend in Dynamical Downscaling of Reanalysis, *J.*
687 *Geophys. Res.*, *115*, D17115. doi: 10.1029/2009JD013511.
- 688 Kessler, R., and S. Douglas (1991), A Numerical Study of Mesoscale Eddy
689 Development over the Santa Barbara Channel, *J. Appl. Meteorol.*, *30*, 633-651.
- 690 Luyten, J. R., D. H. Roemmich (1982), Equatorial Currents at Semi-Annual Period in
691 the Indian Ocean, *J. Phys. Oceanogr.*, *12*, 406-413.

- 692 Mass, C. F. and M. D. Albright (1989), Origin of the Catalina Eddy, *Mon. Wea. Rev.*,
693 *117*, 2406-2436.
- 694 Mass, C. F., and W. J. Steenburgh (2000), An Observational and Numerical Study of an
695 Orographically Trapped Wind Reversal along the West Coast of the United States,
696 *Mon. Wea. Rev.*, *128*(7), 2363.
- 697 Mesinger, F., and Coauthors (2010), North American Regional Reanalysis, *Bull. Amer.*
698 *Meteor. Soc.*, *87*, 343-360. doi:10.1175/BAMS-87-3-343.
- 699 Reason, C. J. C. and D. G. Steyn (1992), The Dynamics of Coastally Trapped
700 Mesoscale Ridges in the Lower Atmosphere, *J. Atmos. Sci.*, *49*, 1677-1692.
- 701 Skamarock, W. C., R. Rotunno, and J. B. Klemp (2002), Catalina Eddies and Coastally
702 Trapped Disturbances, *J. Atmos. Sci.*, *59*(14), 2270-2278. doi: 10.1175/1520-
703 0469(2002)059<2270:CEACTD>2.0.CO;2.
- 704 Small, I. J. (1999), An Observational Study of a California Bight Coastal Convergence
705 Zone Produced by Flow Interaction with Mainland Topography: Precipitation
706 Producer in Southern California, *Western Region Technical Attachment*, (No. 99-
707 19). Retrieved from <http://www.wrh.noaa.gov/wrh/99TAs/9919/index.html>.

- 708 Thompson, W. T., S. D. Burk, and J. Rosenthal (1997), An Investigation of the Catalina
709 Eddy, *Mon. Wea. Rev.*, *125*(6), 1135. doi: 10.1175/1520-
710 0493(1997)125<1135:AIOTCE>2.0.CO;2.
- 711 Ueyoshi, K., and J. Roads (1993), Simulation and Prediction of the Catalina Eddy, *Mon.*
712 *Wea. Rev.*, *121*, 2975-3000.
- 713 Ulrickson, B. L., J. S. Hoffmaster, J. Robinson and D. Vimont (1995), A Numerical
714 Modeling Study of the Catalina Eddy, *Mon. Wea. Rev.*, *123*, 1364-1373.
- 715 Wakimoto, R. (1987), The Catalina Eddy and its Effect on Pollution over Southern
716 California, *Mon. Wea. Rev.*, *115*, 837-855.
- 717 Willett, C. S., R. R. Leben, and M. F. Lavin (2006), Eddies and Tropical Instability
718 Waves in the eastern tropical Pacific: A review, *Prog. Oceanogr.*, *69*(2-4), 218-
719 238. doi: 10.1016/j.pocean.2006.03.010.
- 720
- 721
- 722

723 **Figure Captions**

724

725 Figure 1. Major topographical features and names of the main cities over the Southern
726 California Bight region. The features referenced in the paper are shown in bold and
727 underlined.

728

729 Figure 2. A composite of 15 events for the relative vorticity and streamlines. The
730 composite near-surface structure of the eddy is characterized by elongated positive
731 vorticity emanating from Point of Conception, with a narrow band of negative vorticity
732 along the coast.

733

734 Figure 3. Composites of the CE events for correlation threshold of 0.9 (upper left
735 panel) to 0.2 (lower right panel) in 0.1 intervals. Vorticity contour is shown in red.

736

737 Figure 4. PDF of the duration (hours) of CE events as measured by meridional velocity
738 greater than 1.4 m/s for Scripps Station located at 32.867N 117.257W (blue) and
739 CaRD10 wind in San Diego (magenta).

740

741 Figure 5. (a) Annual Cycle, (b) intensity, (c) average duration (d) PDF of duration (e)
742 PDF of the Hours when CE was present/Diurnal cycle.

743

744 Figure 6. Evolution of 10-meter wind streamline and vorticity (shading) for 00 UTC
745 April 30, to 21 UTC May 2, 2000. Note the complete disappearance of cyclonic
746 circulation at 00 UTC (top row, first, third and 5th columns) and 03 UTC (same
747 columns). Approximate location of San Diego is shown by white circle on the top left
748 panel.

749

750 Figure 7. Another example of dissipating eddy but with surface observation plotted.

751

752 Figure 8. 500 and 850 hPa geopotential height anomaly composite of the mature phase
753 of CE events (a) and (b) and 500 and 850 hPa geopotential height field composite of the
754 mature phase of CE events (c) and (d).

755

756 Figure 9. Vorticity and wind anomalies at 10 m (left panel), and 925 hPa (right panel)
757 for the composite of the mature phase of CE events.

- 758
759 Figure 10. Composite anomaly of divergence at 10 m (left) and temperature at 2 m.
760 The temperature map is overlaid by topography contours (in white).
761
- 762 Figure 11. Composite anomaly of specific humidity (left) and relative humidity (right).
763
- 764 Figure 12. Composite anomaly of latent heat flux (left) and wind speed.
765
- 766 Figure 13. Composite surface pressure.
767
- 768 Figure 14. Composite cross section of temperature anomaly (left) and vorticity (right).
769 The center of the eddy is indicated by a triangle.
770
- 771 Figure 15. 500 hPa and 850 hPa geopotential height fields at 21, 18, 15, 12, 9, 6, 3, and
772 1 hours before the detection of CE event.
773
- 774 Figure 16. Anomaly streamline and vorticity at 21, 18, 15, 12, 9, 6, 3, and 1 hours
775 before the detection of CE event.
776
- 777 Figure 17. Vorticity budget at 10 m above ground at 21, 12, 6 and 1 hour prior to the
778 recognition phase. T_3 is a stretching term, T_1+T_2 is the horizontal advection term and
779 T_0 is a local time change or the storage term.
780
- 781 Figure 18. Near-surface wind vector at initial stages of the eddy formation. Shading is
782 for the east-west component of the wind highlighting the development of the offshore
783 wind (cold colors).
784
- 785 Figure 19. Composite evolution of near-surface air temperature anomaly during the
786 initial phase.
787
- 788 Figure 20. Hourly variation of surface pressure anomaly during the initiation phase of
789 the CE obtained from composite.
790
- 791 Figure 21. Illustration of the CE life cycle. Horizontal axis is time in local Pacific
792 Standard Time.
- 793 Figure 22. Comparison of two CE indices; I2.1 Monthly averages of vorticity averaged

794 over the CE region and I2.2 Monthly averages of winds correlations averaged over the
795 CE region. The correlation between the two indices was 0.75.

796

797 Figure 23. Temporal spectra of vorticity averaged over the Southern California Bight
798 region (32°N – 34°N, 121° W- 117° W).

799

800 Figure 24. Regression of the CE index onto NCEP/NCAR reanalysis monthly mean
801 500 hPa height (top) and near-surface temperature (bottom).

802

803

804

805

806

807

808

809

810

811

812

Table 1: Hit and miss occurrences with respect to CE detected by MA for May-September 1968-1982

Init Date	InitHour	Model InHour	End Date	EndHour	Model Dur
1968-05-01-21	2925	2918/2929	1968-05-02-21	2949	4HH;1HH
1968-05-27-09	3537	3536/3558	1968-05-29-03	3579	8HH;3HH
1968_06-23-15	4191	4183	1968-06-25-18	4242	11HH;
1968-06-28-18	4314	N/A	1968-06-30-21	4365	N/A
1969-06-15-15	3975	3976/3997	1969-06-17-21	4029	7HH/10HH
1969-06-23-21	4173	4163/4186	1969-06-26-18	4242	11HH/1HH
1970-06-12-00	3888	3878/3948	1970-06-14-00	3936	3hh/4hh
1970-06-28-12	4284	4288/4309	1970-06-29-21	4317	4HH/5HH
1970-09-11-18	6090	N/A	1970-09-13-06	6126	N/A
1971-05-05-21	2997	2993	1971-05-07-06	3030	3HH
1971-09-01-06	5838	5840	1971-09-03-06	5886	8HH
1972-07-14-06	4686	4688	1972-07-16-09	4737	2HH
1972-08-02-06	5142	5144/5154	1972-08-04-00	5184	8HH/2HH
1972-08-17-18	5514	5507	1972-08-19-15	5559	6HH
1972-08-23-06	5646	5646/5654/5670	1972-08-26-00	5712	7HH/2HH/9HH
1972-09-05-06	5958	N/A	1972-09-07-06	6006	N/A
1972-09-22-21	6381	N/A	1972-09-25-09	6441	N/A
1973-05-04-09	2961	2969	1973-05-05-09	2985	6HH
1973-06-13-12	3924	3930	1973-06-15-00	3960	8HH
1973-08-25-03	5667	5671/5675	1973-08-26-15	5703	2HH/9HH
1973-09-07-06	5982	5994/6005	1973-09-10-00	6048	2HH/3HH
1974-05-14-15	3207	3204/3224	1974-05-16-00	3240	10HH/12HH
1974-06-06-06	3750	3792/3796	1974-06-09-03	3819	2HH/5HH
1974-08-18-12	5508	5506/5530/5552	1974-08-21-06	5574	3hh/8HH/3HH
1975-07-12-06	4614	4618/4641/4669	1975-07-14-15	4671	9HH/3HH/1HH
1976-05-02-06	2934	2937/2947	1976-05-04-09	2985	7HH/1HH
1976-09-15-00	6192	6185/6202	1976-09-16-09	6225	3HH/2HH
1977-05-04-09	2961	2968/2984	1977-05-06-03	3003	3HH/11HH
1977-07-22-18	4866	4859/4878/	1977-07-24-06	4902	6HH/2HH
1977-08-17-15	5487	N/A	1977-08-18-09	5505	N/A
1977-08-26-09	5697	5699/5724	1977-08-28-12	5748	9HH/9HH
1978-06-26-09	4233	4231	1978-06-27-03	4251	13HH
1978-09-05-21	5949	N/A	1978-09-06-15	5967	N/A
1979-05-26-21	3501	3505/3541	1979-05-28-00	3528	1HH/6HH
1979-06-05-06	3726	3737/3752/3793	1979-06-08-06	3798	2HH/2HH/3HH
1979-06-17-09	4017	3993	1979-06-18-09	4041	10HH
1979-07-01-09	4353	4355	1979-07-02-21	4389	10HH
1979-07-12-15	4623	4625/4637/	1979-07-14-00	4656	2HH/2HH
1979-07-19-03	4779	4767	1979-07-21-00	4824	4HH
1980-05-07-06	3054	3063/3085	1980-05-08-06	3078	2HH/7HH
1980-06-30-12	4356	4355/4371	1980-07-02-00	4392	7HH/1HH
1980-08-02-12	5148	5147/5177/5199	1980-08-04-15	5199	6HH/1HH/3HH
1980-08-12-12	5388	5410	1980-08-13-21	5421	11HH
1980-09-07-09	6009	N/A	1980-09-08-21	6045	N/A
1981-06-08-12	3804	3808/3875	1981-06-11-12	3876	3HH/5HH
1981-06-17-18	4026	4019	1981-06-19-18	4074	8HH
1981-08-30-12	5796	N/A	1981-09-01-00	5832	N/A
1981-09-22-09	6345	N/A	1981-09-24-00	6384	N/A
1982-05-08-00	3048	N/A	1982-05-09-03	3075	N/A
1982-05-18-00	3288	3280	1982-05-19-09	3321	14HH

Table 2: CE occurrences based on CaRD10 and NARR surface data for May 2005. 75% of CaRD10 CE events were detected in NARR.

CaRD10	NAM
2005 05 04 07	YES
2005 05 05 03	YES
2005 05 05 20	YES
2005 05 14 11	YES
2005 05 16 07	YES
2005 05 20 09	NO
2005 05 23 03	YES
2005 05 24 06	YES
2005 05 27 14	NO
2005 05 28 04	YES
2005 05 29 14	YES
2005 05 31 13	NO

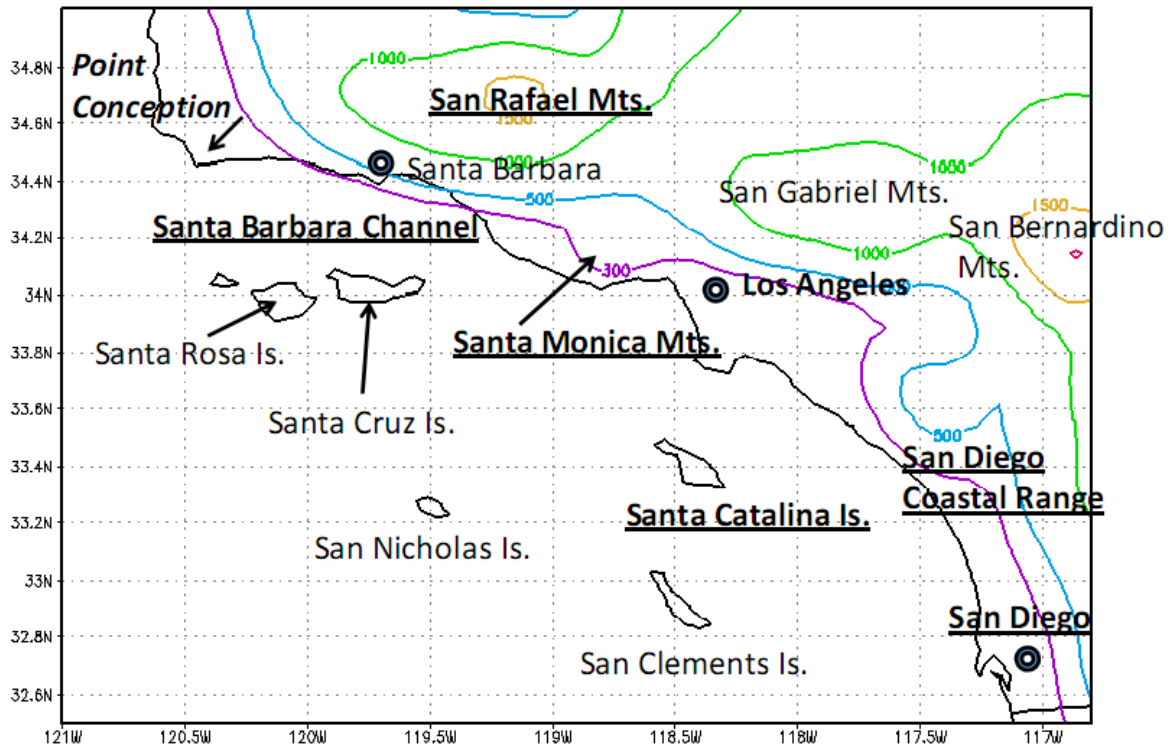


Figure 1. Major topographical features and names of the main cities over the Southern California Bight region. The features referenced in the paper are shown in bold and underlined.

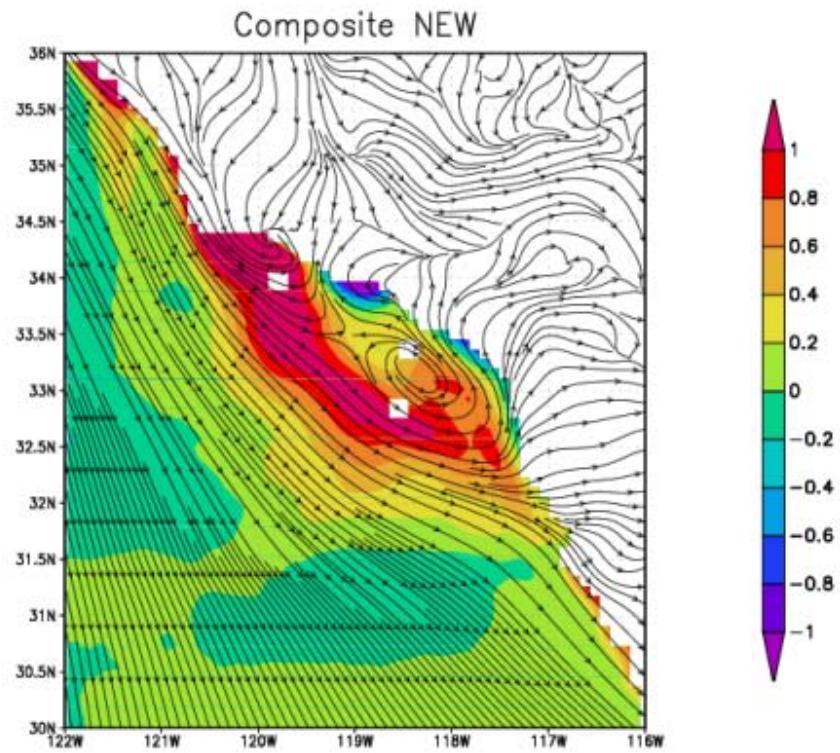


Figure 2. Composite of 15 events for the relative vorticity and streamlines. The composite near-surface structure of the eddy is characterized by elongated positive vorticity emanating from Point of Conception, with a narrow band of negative vorticity along the coast.

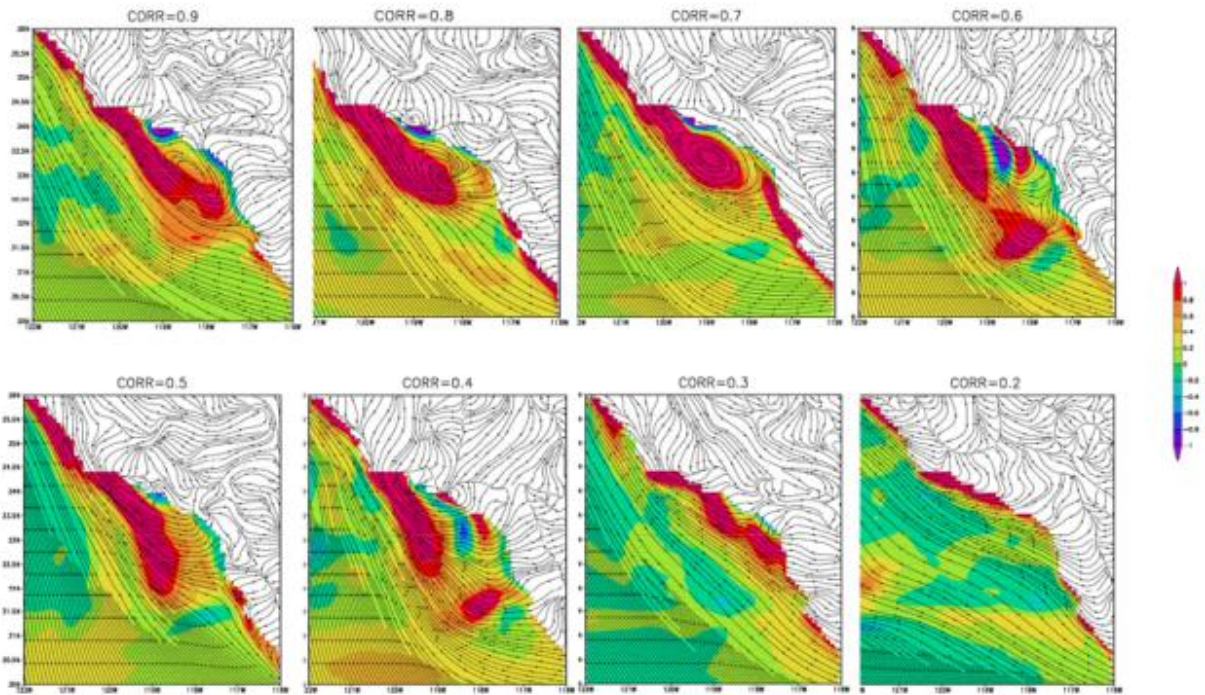


Figure 3. Composites of the CE events for correlation threshold of 0.9 (upper left panel) to 0.2 (lower right panel) in 0.1 intervals. Vorticity contour is shown in red.

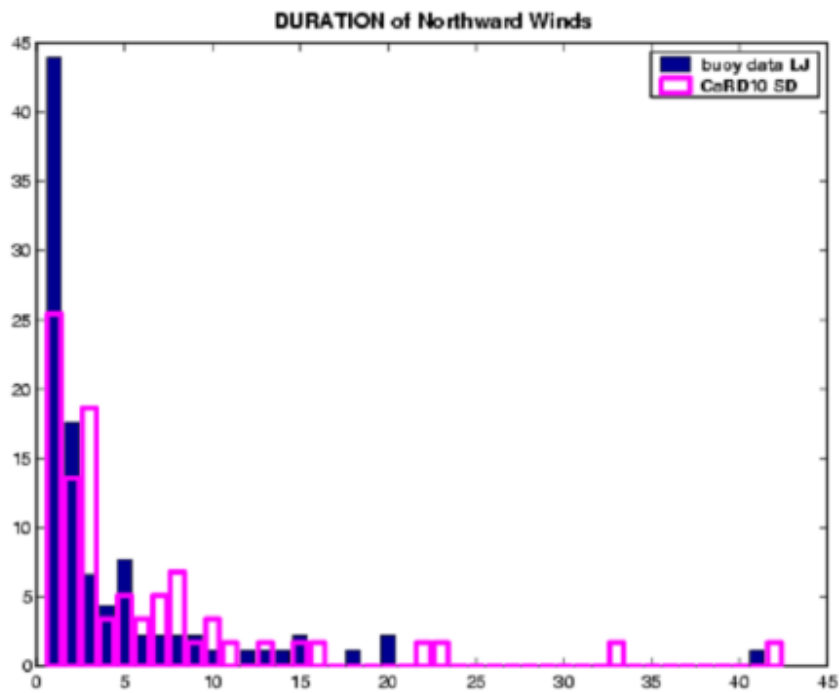


Figure 4. PDF of the duration (hours) of CE events as measured by meridional velocity greater than 1.4 m/s for Scripps Station located at 32.867N 117.257W (blue) and CaRD10 wind in San Diego (magenta)

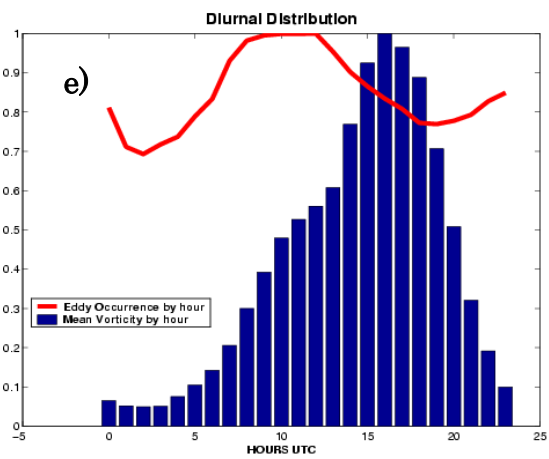
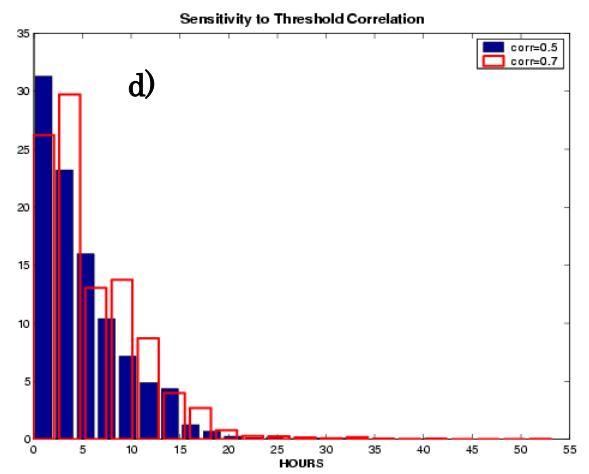
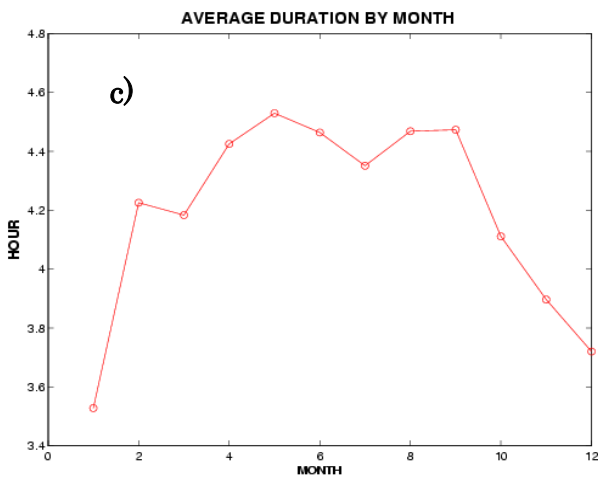
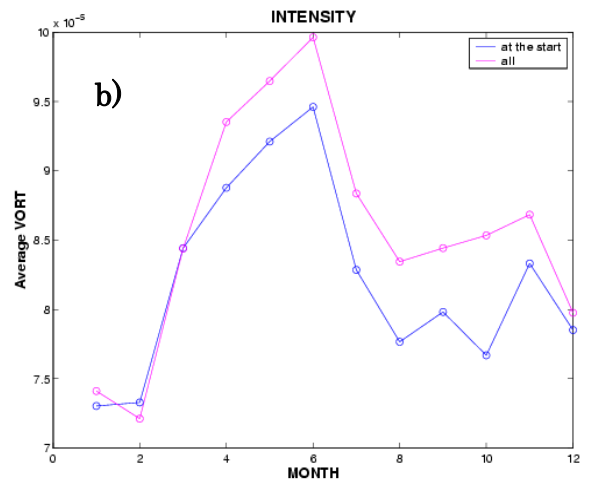
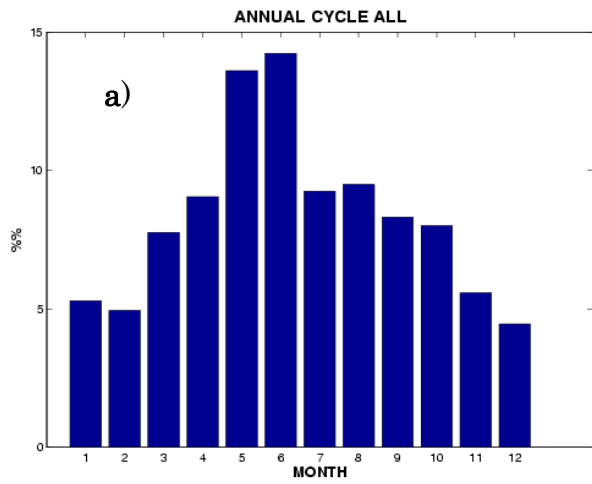


Figure 5. (a) Annual Cycle, (b) intensity, (c) average duration (d) PDF of duration (e) PDF of the Hours when CE was present/Diurnal cycle

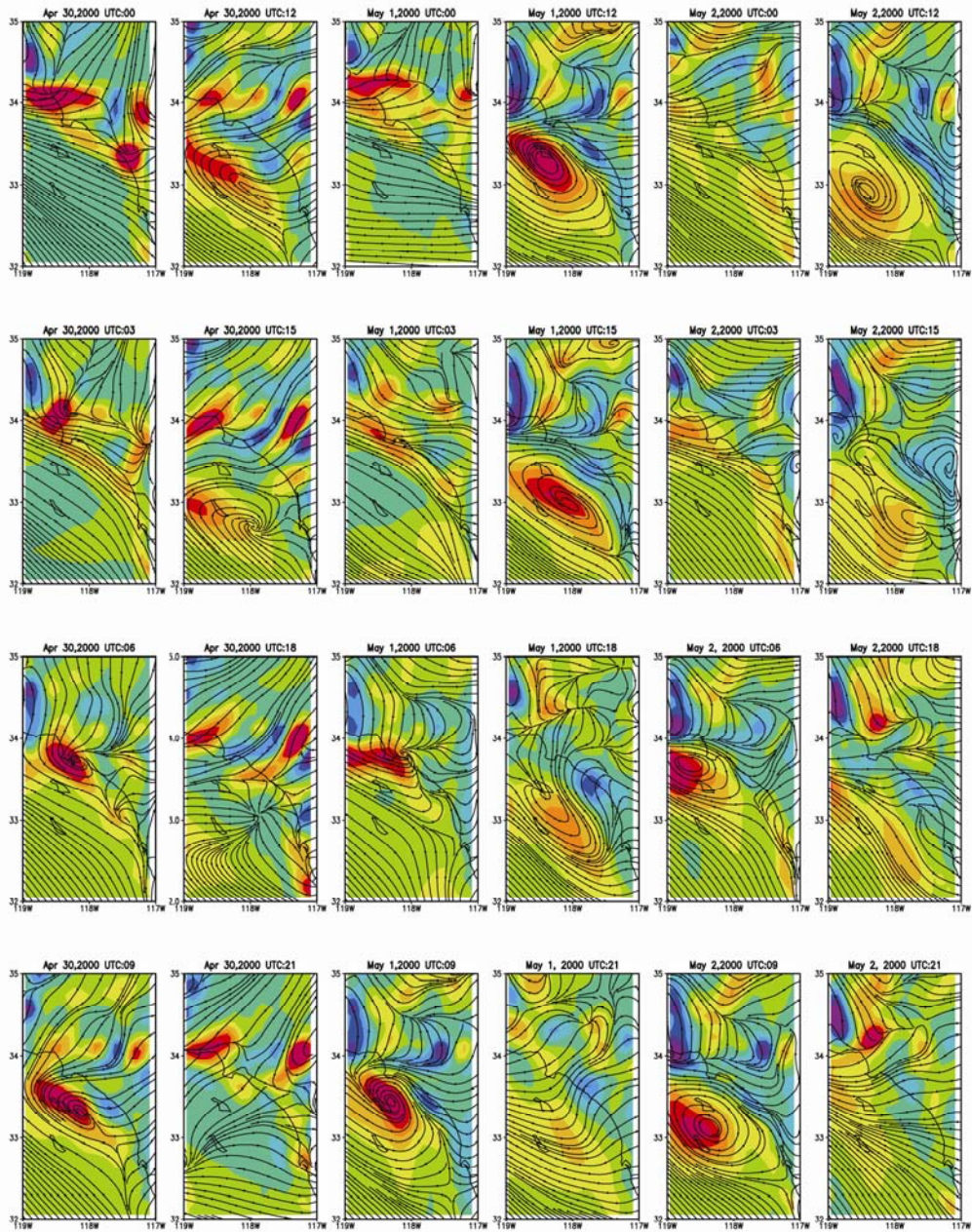


Figure 6. Evolution of 10-meter wind streamline and vorticity (shading) for 00Z April 30, to 21Z May 2, 2000. Note the complete disappearance of cyclonic circulation at 00 Z (top row, first, third and 5th columns) and 03Z (same columns). Approximate location of San Diego is shown by white circle on the top left-most panel.

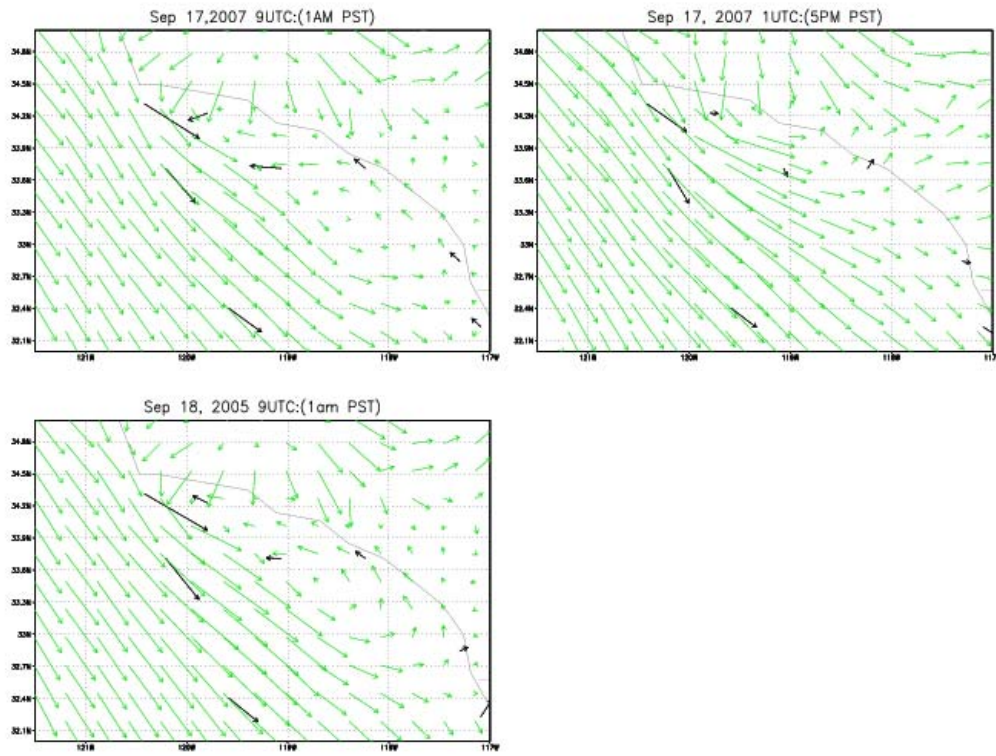


Figure 7. Another example of dissipating eddy but with surface observation plotted.

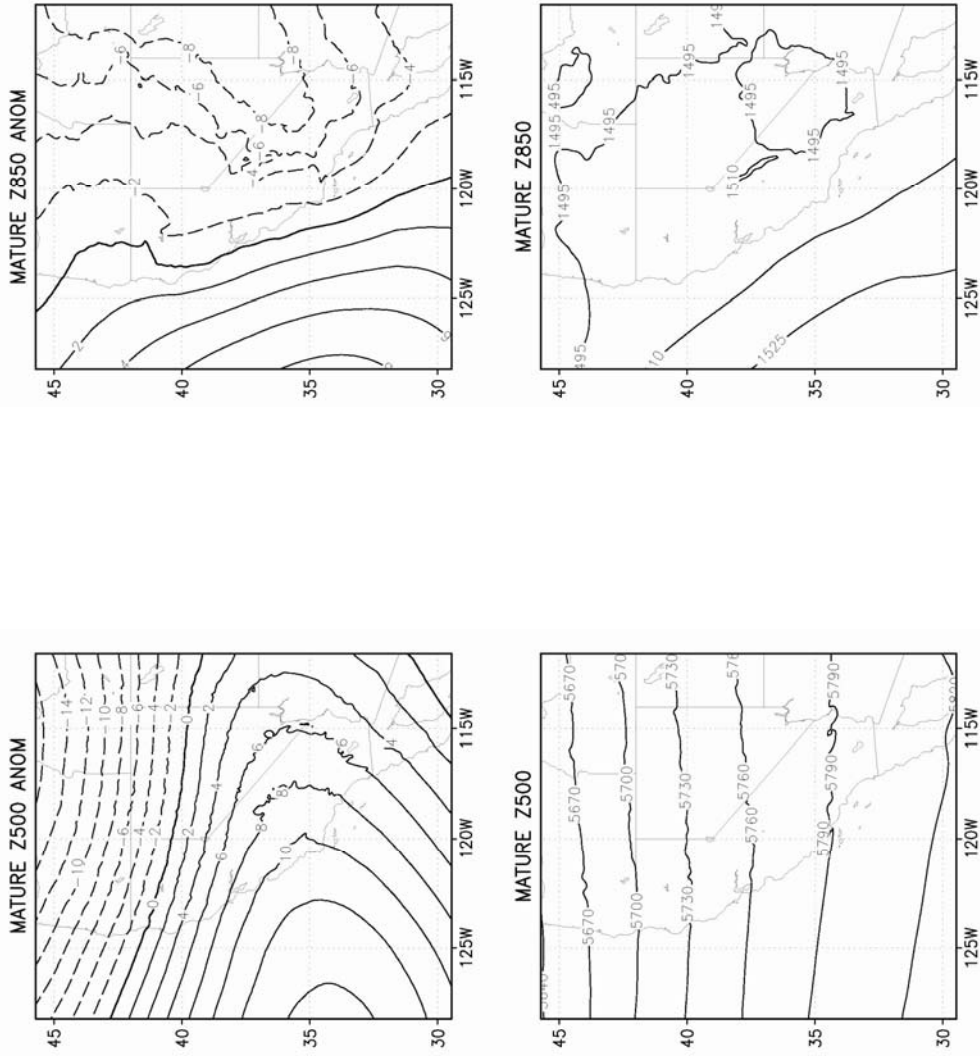


Figure 8. 500 and 850 hPa geopotential height anomaly (top two panels) and full field (bottom two panels) composite of mature phase of CE events.

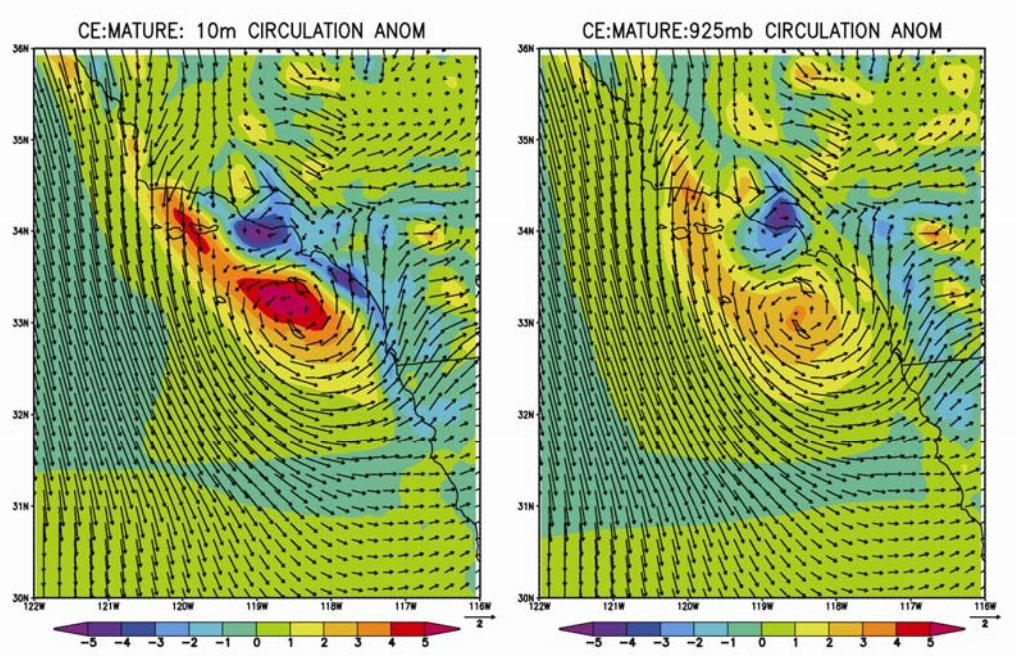


Figure 9. Vorticity and wind anomalies at 10m (left panel), and 925 hPa (right panel) for the composite of the mature phase of CE events.

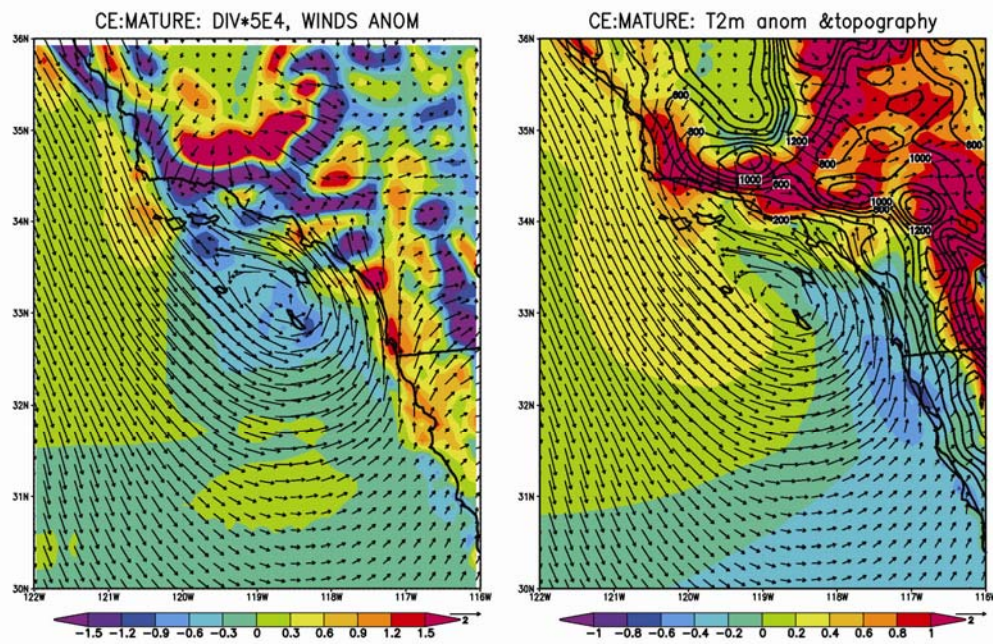


Figure 10. Composite anomaly of divergence at 10m (left) and temperature at 2m. The temperature map is overlaid by topography contours (in thick black lines).

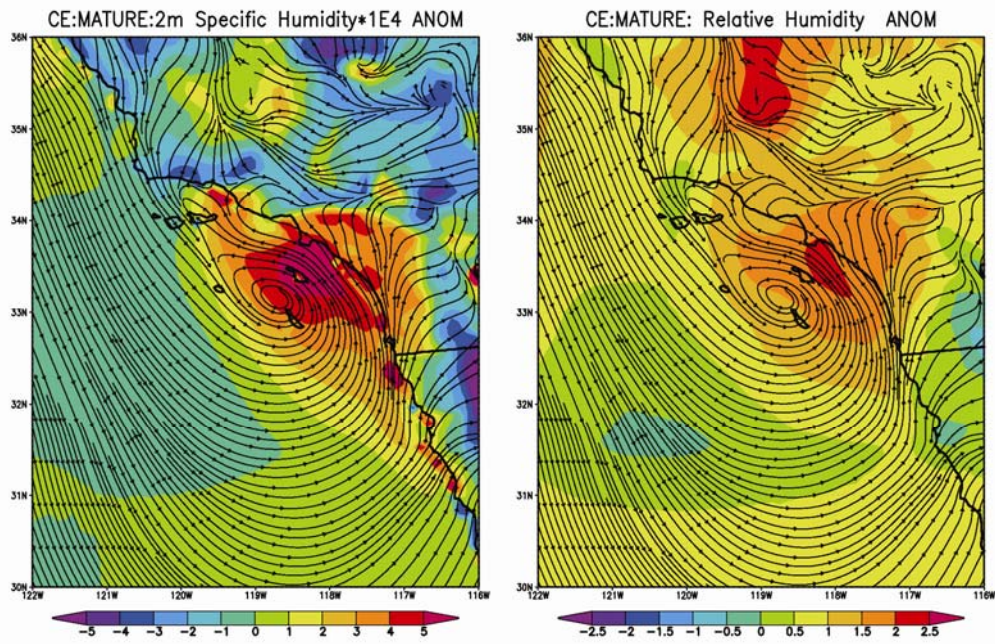
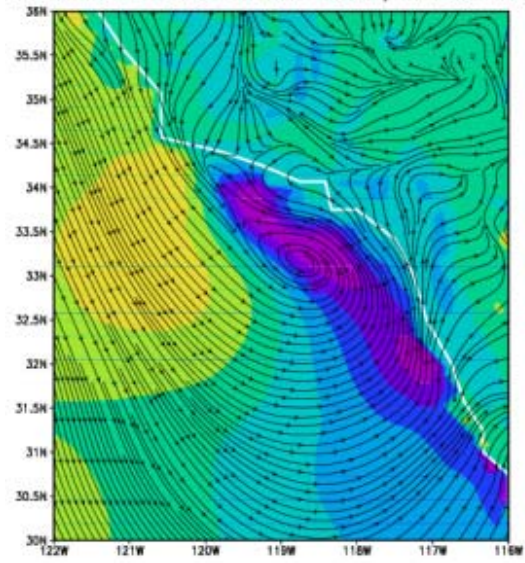


Figure 11. Composite anomaly of specific humidity (left) and relative humidity (right).

CE:MATURE: SFC LATENT HEAT, WND ANOM



CE:MATURE: WND ANOM

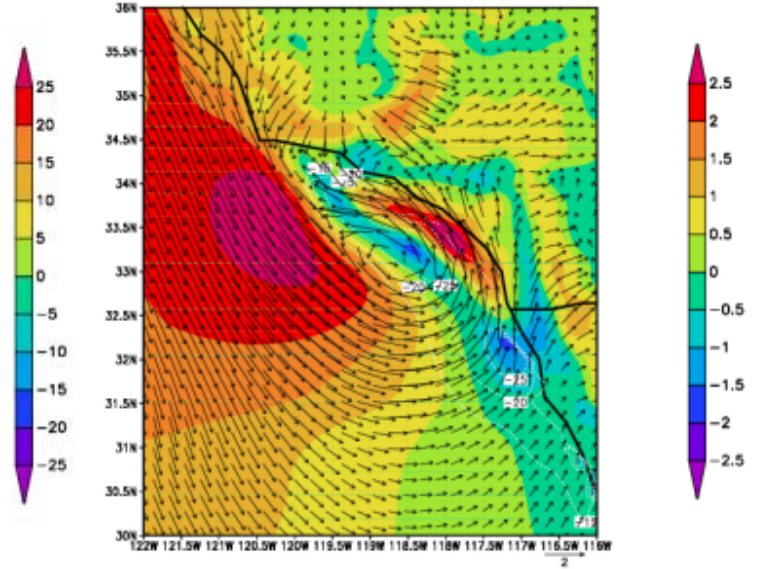


Figure 12. Composite anomaly of latent heat flux (left) and wind speed.

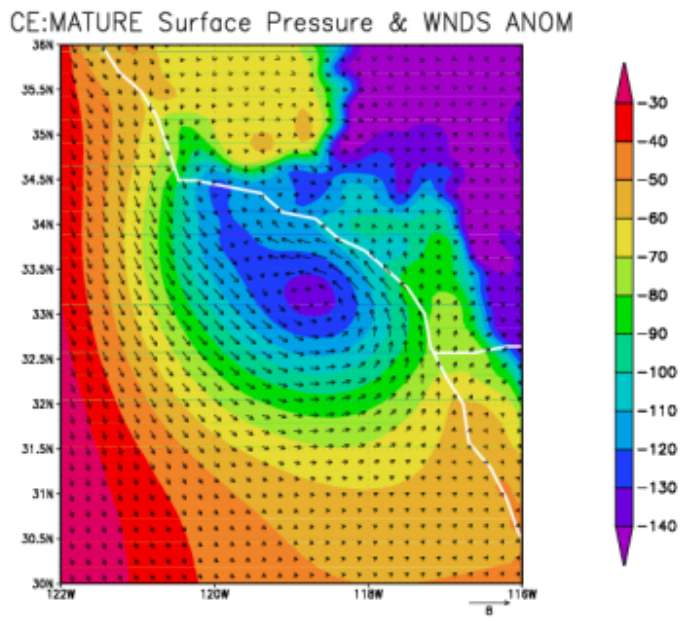


Figure 13. Composite surface pressure.

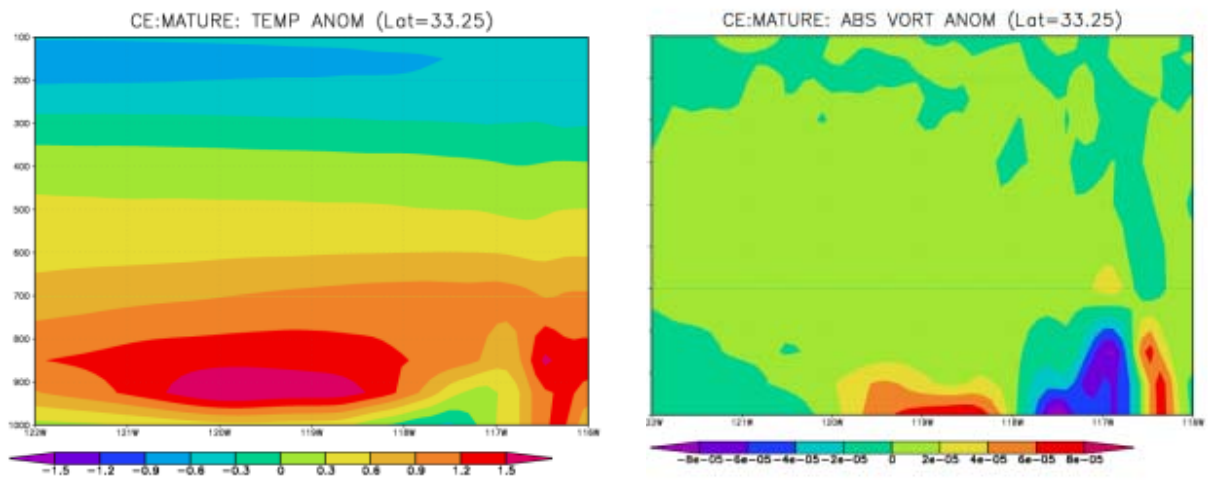


Figure 14. Composite cross section of temperature anomaly (left) and vorticity (right) along east west crossing the eddy center. The center of the eddy is indicated by triangle.

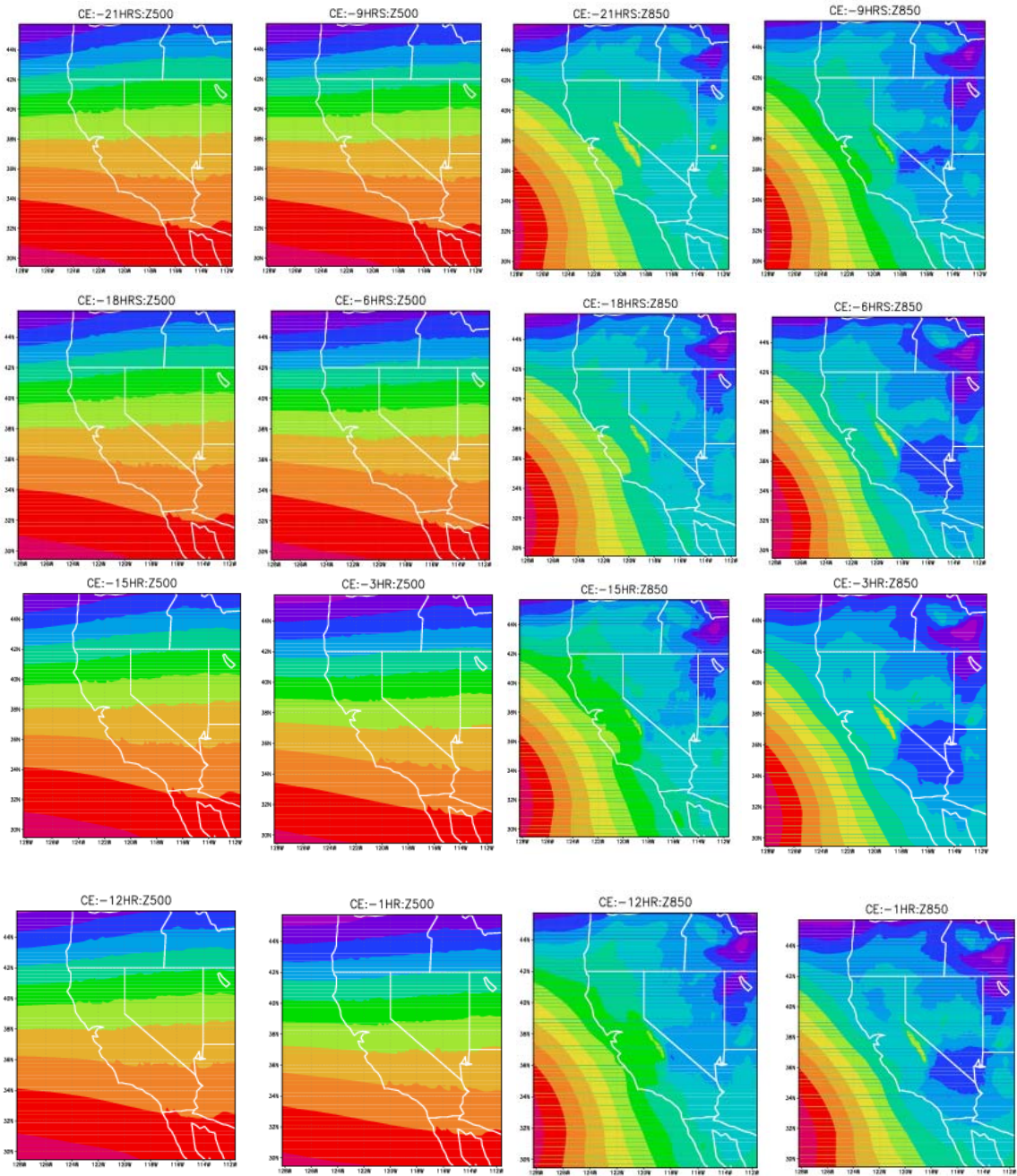


Figure 15. 500 hPa and 850 hPa geopotential height fields at 21, 18, 15, 12, 9, 6, 3, and 1 hours before the detection of CE event

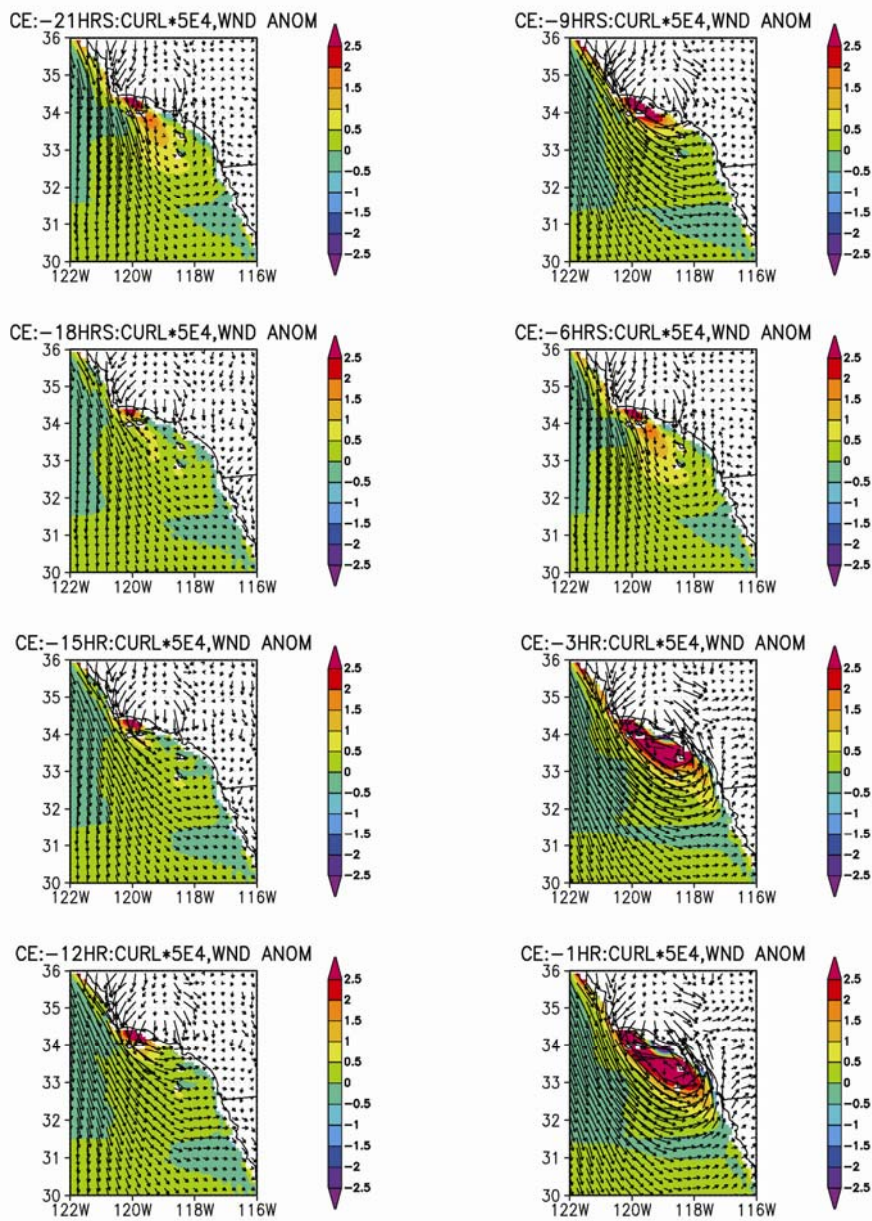


Figure 16. Anomaly wind vector and vorticity at 21, 18, 15, 12, 9, 6, 3, and 1 hours before the detection of CE event

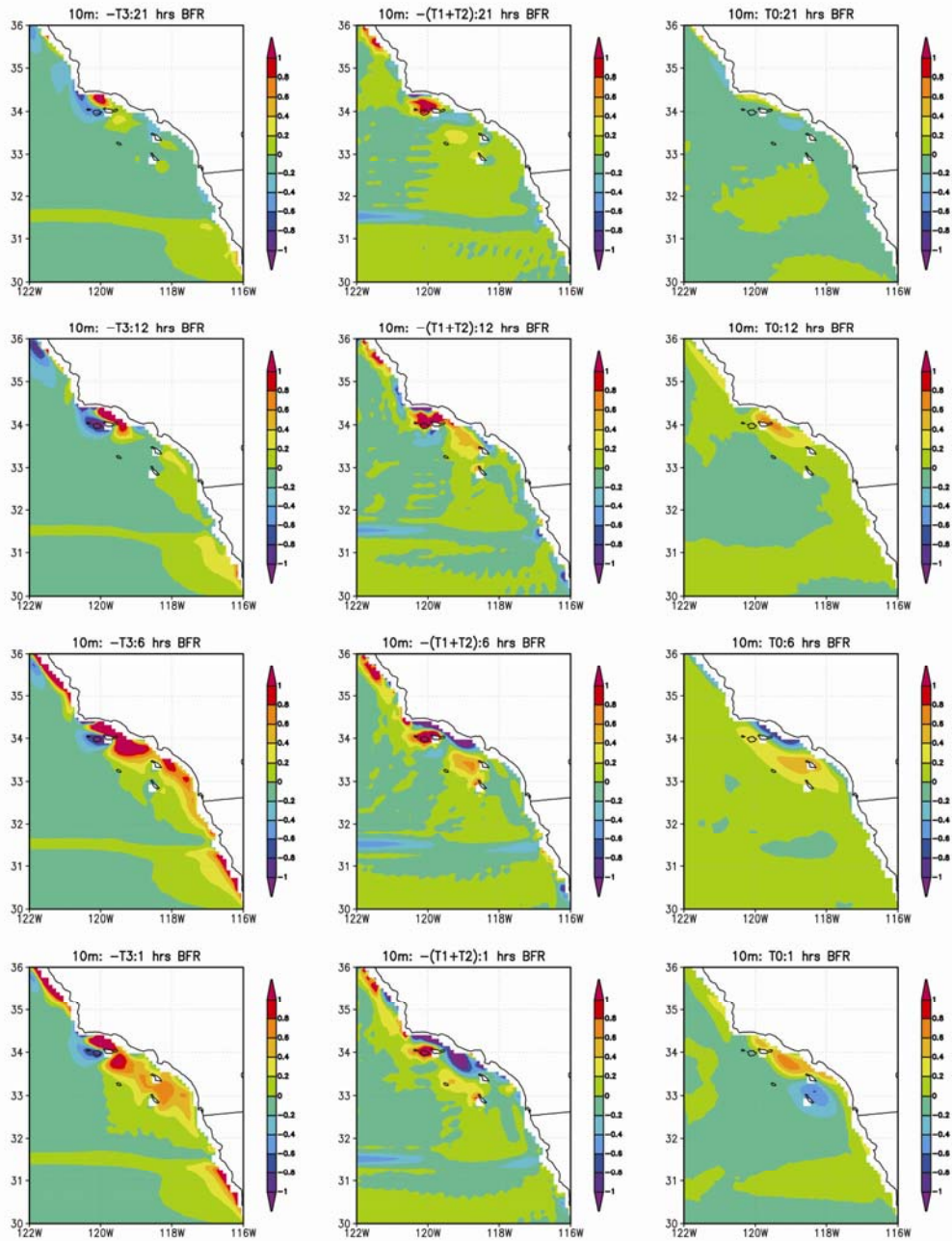


Figure 17. Vorticity budget at 10m above ground at 21, 12, 6 and 1 hour prior to the recognition phase. T_3 is a stretching term, T_1+T_2 is the horizontal advection term and T_0 is a local time change or the storage term.

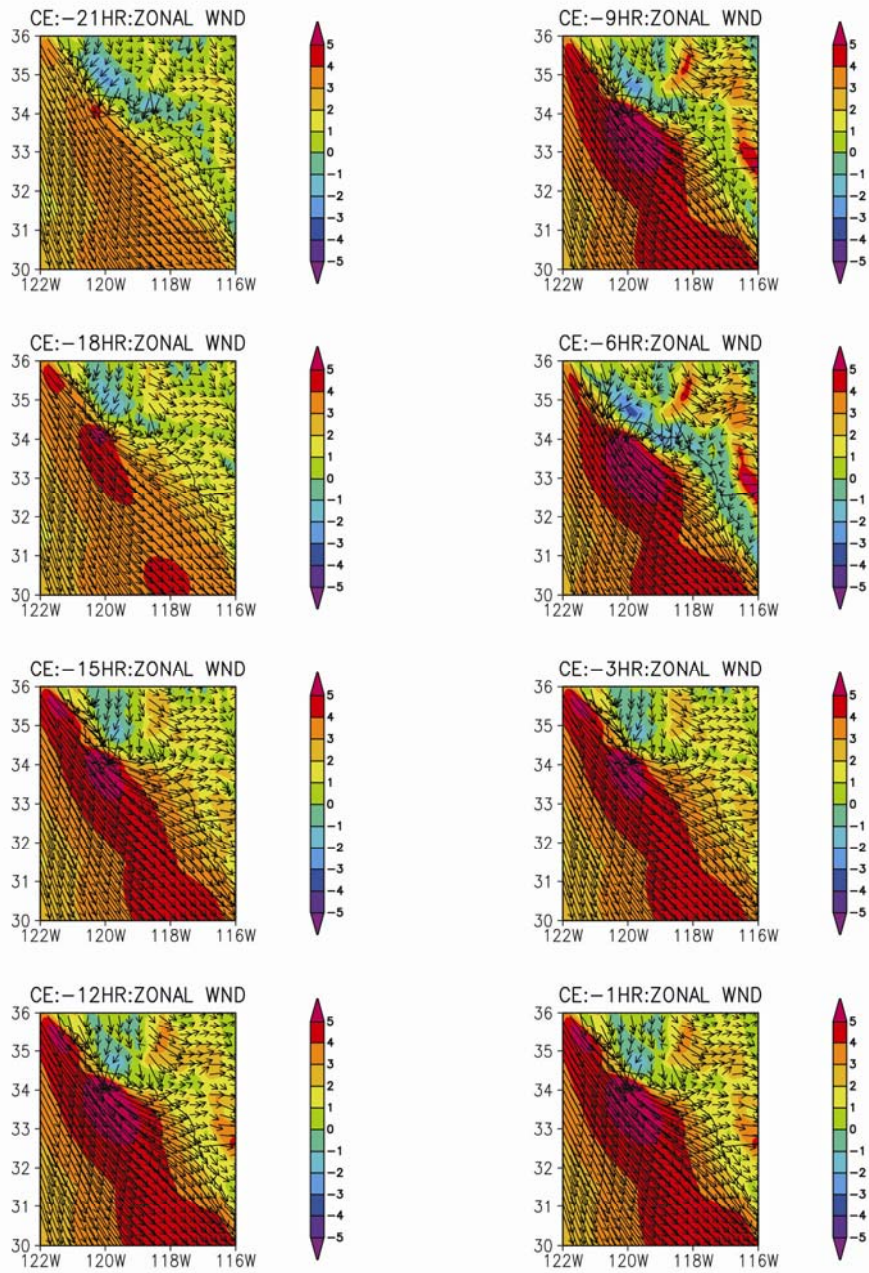


Figure 18. Near surface wind vector at initial stages of the eddy formation. Shading is for the east-west component of the wind highlighting the development of the off shore wind (cold colors).

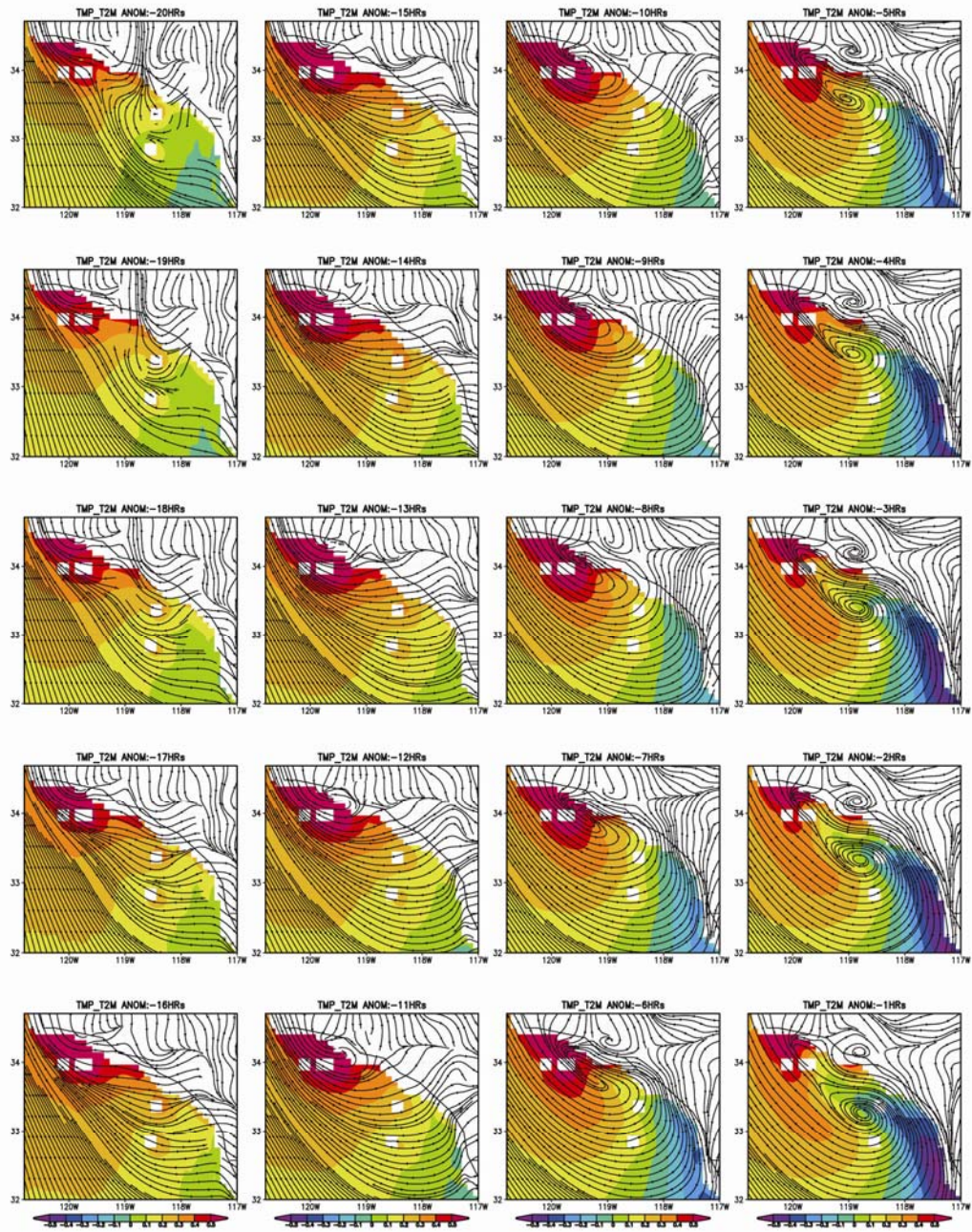


Figure 19. Composite evolution of near surface air temperature anomaly during the initial phase.

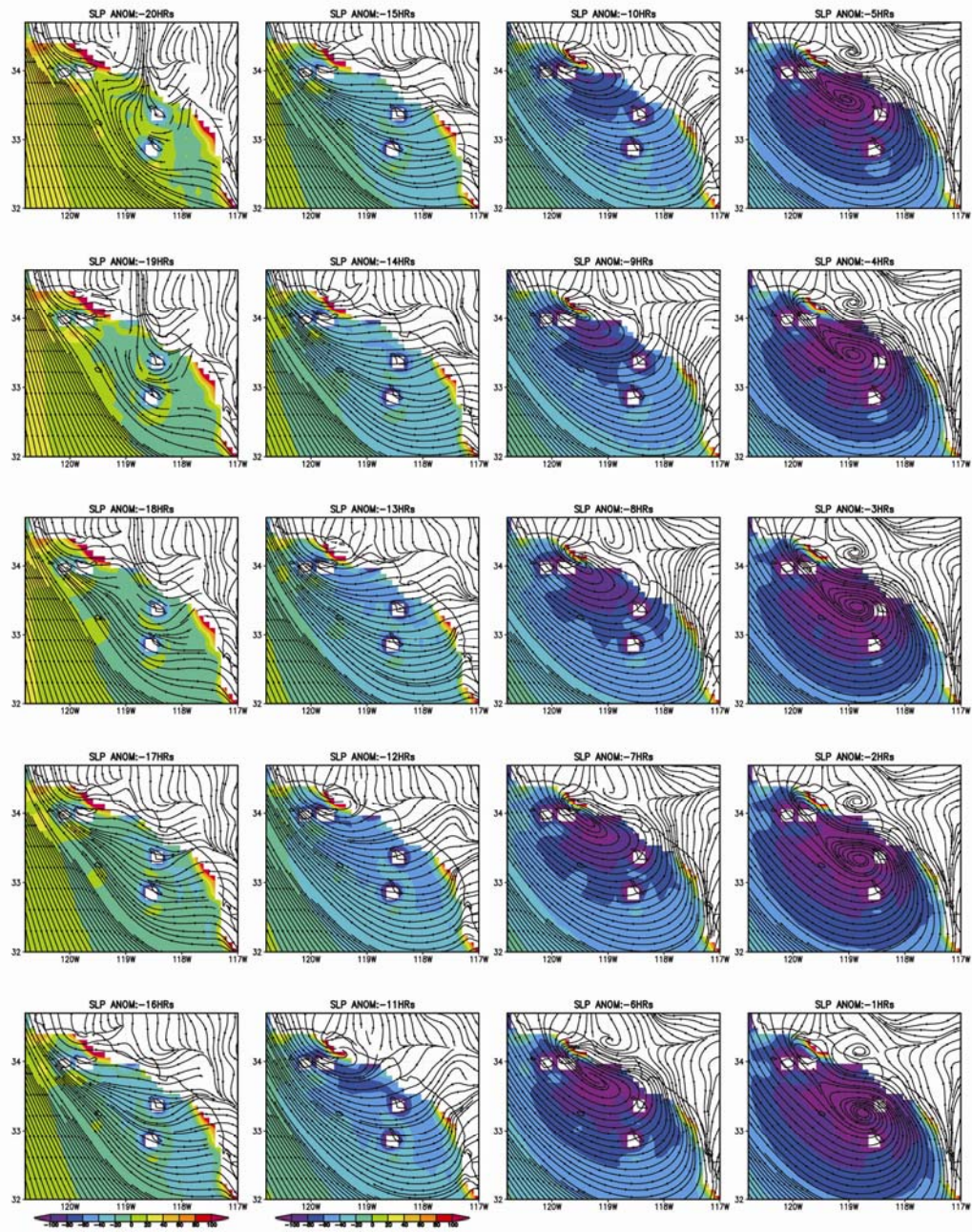


Figure 20. Hourly variation of surface pressure anomaly during the initiation phase of the Catalina eddy obtained from composite.

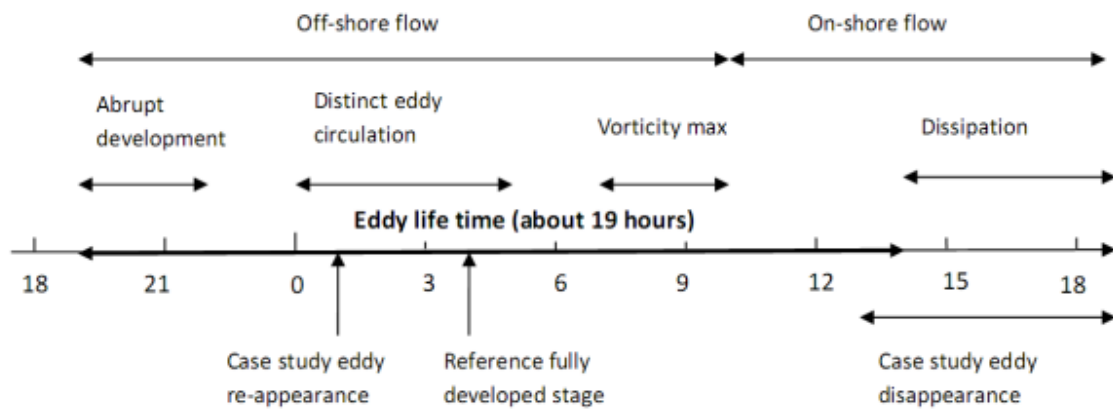


Figure 21. Illustration of the Catalina Eddy life cycle. Horizontal axis is time in local Pacific Standard Time.

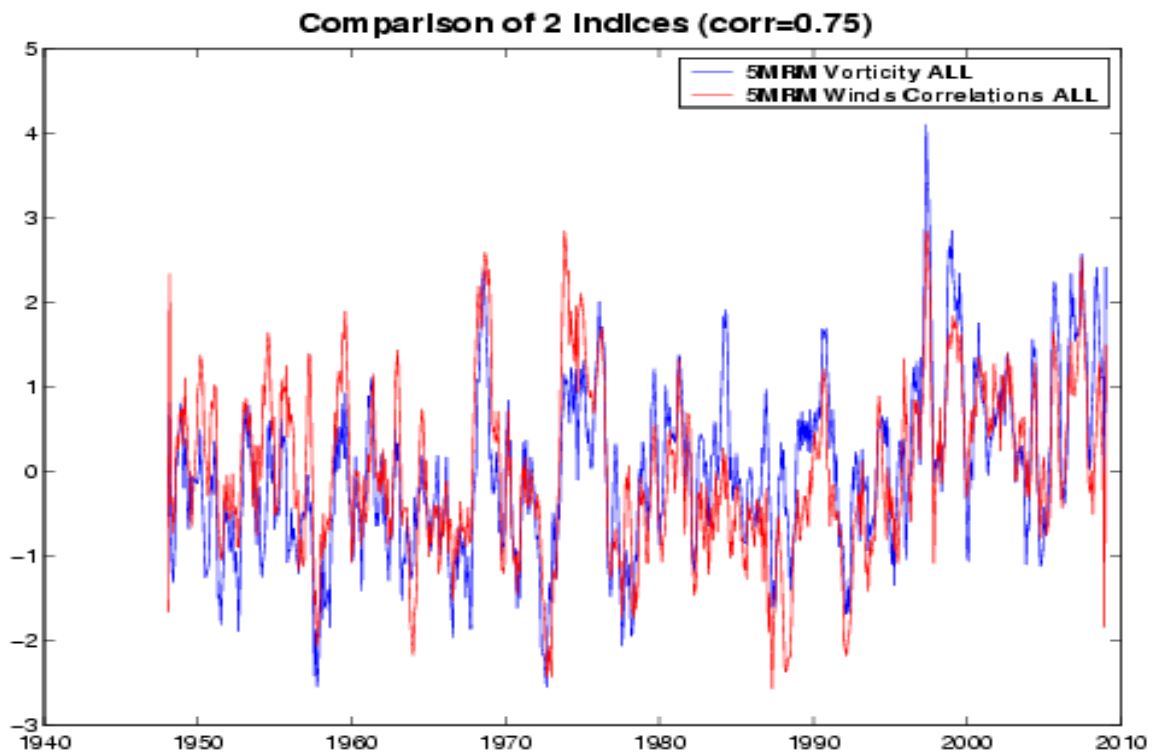


Figure 22. Comparison of two CE indices; I2.1 Monthly averages of Vorticity averaged over CE region and I2.2 Monthly averages of Winds Correlations averaged over CE region. The correlation between the two indices was 0.75.

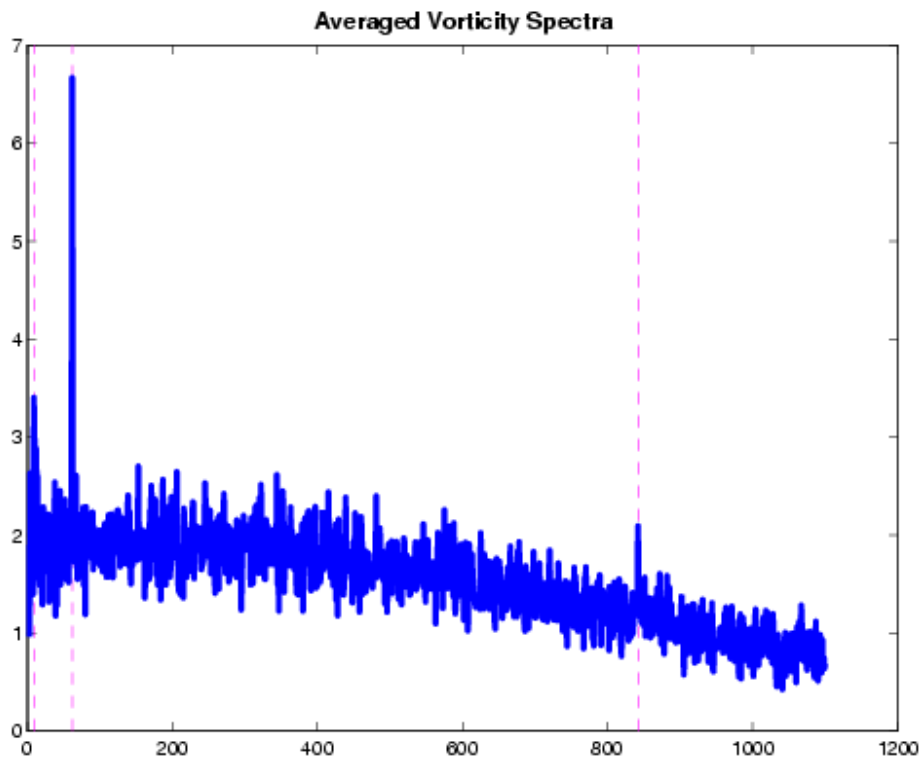
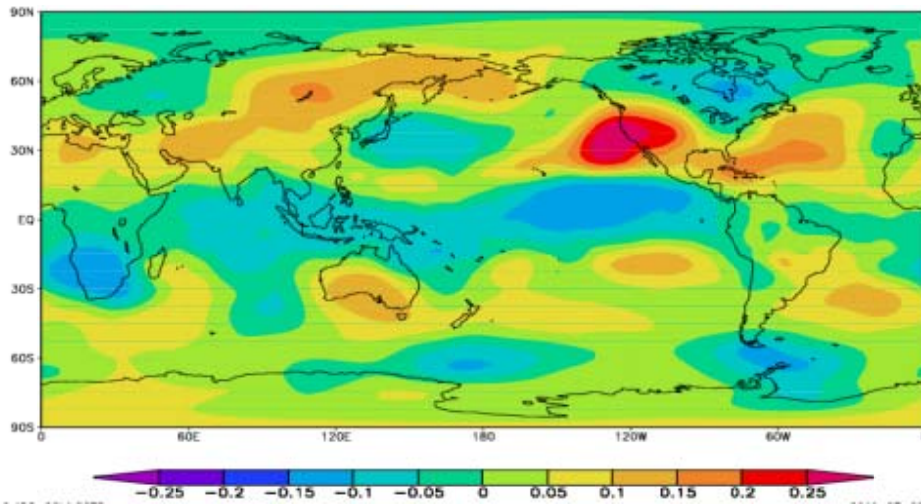


Figure 23. Temporal spectra of vorticity averaged over the Southern California Bight region ($32^{\circ}\text{N} - 34^{\circ}\text{N}$, $121^{\circ}\text{W} - 117^{\circ}\text{W}$).

**Regression of CE index onto R-2
monthly Z500 (1970-2008)**



**Regression of CE index onto R-2 monthly T2m
(1970-2008)**

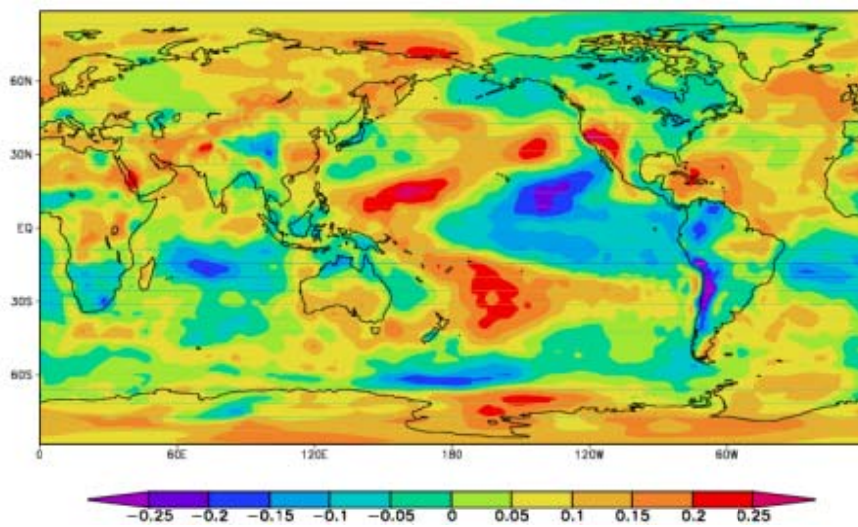


Figure 24. Regression of CE index onto NCEP/NCAR reanalysis monthly mean 500 hPa height (top) and near surface temperature (bottom).